

AD-A163 946

HIGH RESOLUTION COHERENT ANTI-STOKES RAMAN SPECTROSCOPY 1/1

OF DEUTERIUM GAS(U) AIR FORCE INST OF TECH

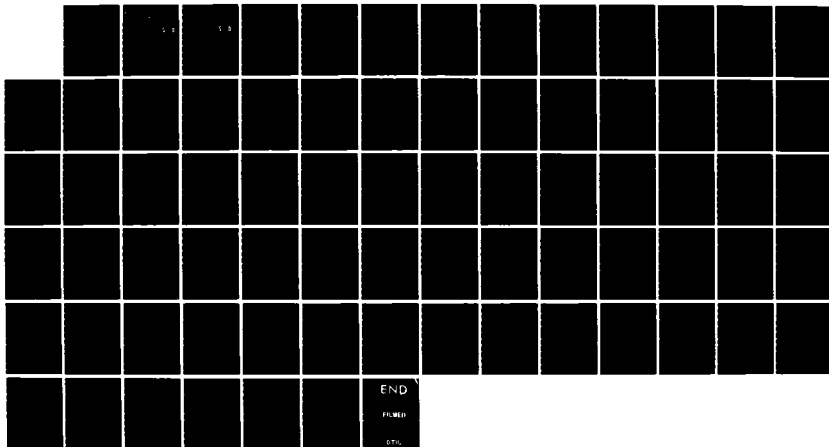
WRIGHT-PATTERSON AFB OH SCHOOL OF ENGI.. D A RUSSELL

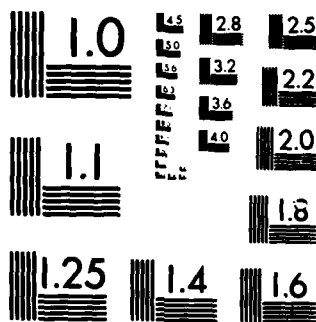
UNCLASSIFIED

DEC 85 AFIT/GEO/ENP/85D-4

F/G 7/4

NL





MICROCOPY RESOLUTION TEST CHART
NATIONAL BUREAU OF STANDARDS 1963-A

AD-A163 946



DTIC
ELECTE
FEB 12 1986
S D

HIGH RESOLUTION COHERENT ANTI-STOKES
RAMAN SPECTROSCOPY OF DEUTERIUM GAS

THESIS

David A. Russell
Second Lieutenant, USAF

AFIT/GEO/ENP/85D-4

DISTRIBUTION STATEMENT A

Approved for public release;
Distribution Unlimited

DEPARTMENT OF THE AIR FORCE

AIR UNIVERSITY

AIR FORCE INSTITUTE OF TECHNOLOGY

Wright-Patterson Air Force Base, Ohio

FILE COPY

AFIT/GEO/ENP/85

DTIC
ELECTE
FEB 12 1986
S D D

HIGH RESOLUTION COHERENT ANTI-STOKES
RAMAN SPECTROSCOPY OF DEUTERIUM GAS

THESIS

David A. Russell
Second Lieutenant, USAF

AFIT/GEO/ENP/85D-4

Approved for public release; distribution unlimited

AFIT/GEO/ENP/85D-4

HIGH RESOLUTION COHERENT ANTI-STOKES
RAMAN SPECTROSCOPY OF DEUTERIUM GAS

THESIS

Presented to the Faculty of the School of Engineering
of the Air Force Institute of Technology

Air University

In partial Fulfillment of the
Requirements for the Degree of
Master of Science in Electrical Engineering



David A. Russell, B.S.
Second Lieutenant, USAF

December 1985

Accession For	
NTIS CRA&I	<input checked="checked" type="checkbox"/>
DTIC TAB	<input type="checkbox"/>
Unannounced	<input type="checkbox"/>
Justification	
By	
Distribution	
Availability Codes	
Dist	Avail and/or Special
A-1	

Approved for public release; distribution unlimited

Preface

This research project was designed to acquire new and more accurate information about the Q-branch transitions of deuterium. At the same time, the coherent anti-Stokes Raman spectroscopy system here at the AFIT School of Engineering was improved and refined. I selected this thesis to gain first hand experience in an experimental laboratory and to learn what complications are involved. I am pleased to have achieved each of these goals.

I would like to thank Dr. Won B. Roh for proposing this topic and for being my faculty advisor. I sincerely appreciate his countless hours of assistance. I am also deeply grateful to Lieutenant Gary Beatovich for reading and commenting on the rough draft. Finally, I owe a word of thanks to the AFIT Fabrication Shop for machining the parts for the gas handling system.

David A. Russell

Table of Contents

	Page
Preface	ii
List of Figures	iv
List of Tables	v
List of Symbols	vi
Abstract	viii
I. Introduction	1
II. Theory	4
Nonlinear Polarization	6
Generation of the Anti-Stokes Wave	8
Susceptibility	11
Linewidth Dependence on Pressure	14
Transition Frequencies	15
III. Experimental Equipment	18
Lasers	18
Diagnostic Equipment	20
Gas Handling System	22
Detection Equipment	22
IV. Procedures	24
Experimental Procedure	24
Analytical Procedure	27
V. Results	29
VI. Analysis	37
Linewidth Analysis	37
Transition Frequency Analysis	47
VII. Conclusions and Recommendations	57
Bibliography	59
Vita	62

List of Figures

Figure	Page
1. The CARS Process	5
2. Block Diagram of the CARS System	19
3. Sample Linewidth Strip Chart Recording	35
4. Sample Frequency Strip Chart Recording	36
5. Q(0) Linewidth vs Density	38
6. Q(1) Linewidth vs Density	39
7. Q(2) Linewidth vs Density	40
8. Q(3) Linewidth vs Density	41
9. Q(4) Linewidth vs Density	42
10. Linewidth of all Transitions vs Density	44
11. Q(0) Transition Frequency vs Density	49
12. Q(1) Transition Frequency vs Density	50
13. Q(2) Transition Frequency vs Density	51
14. Q(3) Transition Frequency vs Density	52
15. Q(4) Transition Frequency vs Density	53

List of Tables

Table	Page
I. Dunham Coefficients for Deuterium	17
II. Deuterium Transition Frequencies	17
III. Lowest Pressure with an Observable AS Signal. .	29
IV. Linewidth and Transition Frequencies of Q(0). .	31
V. Linewidth and Transition Frequencies of Q(1). .	31
VI. Linewidth and Transition Frequencies of Q(2). .	32
VII. Linewidth and Transition Frequencies of Q(3). .	32
VIII. Linewidth and Transition Frequencies of Q(4). .	33
IX. Usual Maximum Photon Counts	34
X. Pressure Broadening and Self Diffusion Coefficients.	46
XI. Transition Frequencies	48
XII. Frequency Shift Coefficients	55

List of Symbols

Symbol	Description	First Reference
a	Pressure broadening coefficient	15
A	Amplitude of the electric field	7
A^*	Complex conjugate of A	8
A_{AS}	Amplitude of the AS electric field	9
A_p	Amplitude of the pump electric field	7
A_s	Amplitude of the Stokes electric field	7
AS	Anti-Stokes	4
b	Frequency shift coefficient	47
c	Speed of light in vacuum	9
C	A constant	11
c.c.	Complex conjugate	7
CARS	Coherent anti-Stokes Raman spectroscopy	1
D_0	Self diffusion coefficient	15
e^p	$\exp[i(k_p z - \omega_p t)]$	8
e^s	$\exp[i(k_s z - \omega_s t)]$	8
E	Electric field	6
E_p	Pump electric field	7
E_s	Stokes electric field	7
F	Molecular driving force	12
H	Interaction energy	12
k_{AS}	Anti-Stokes propagation vector	9
k_p	Pump propagation vector	7
k_s	Stokes propagation vector	7
m	Reduced mass of molecule	12
P	Polarization	6

$P^{(L)}$	Linear component of polarization	6
$P^{(NL)}$	Nonlinear component of polarization	6
$P^{(3)}$	Third order component of polarization	7
P_{CARS}	CARS polarization	8
P_{AS}	Anti-Stokes power	11
q_0	Average molecular spacing	11
$q(t)$	Molecular spacing	11
Q	Amplitude of molecular spacing solution	12
t	Time	7
z	Direction of propagation	7
α	Molecular polarizability	11
α_0	Average molecular polarizability	11
Γ	Linewidth	12
δ	RMS error in curve fitting	45
Δk	Propagation vector mismatch	10
$\Delta \nu$	Linewidth	15
ϵ_0	Permittivity of vacuum	6
λ	Transition wavelength in vacuum	15
μ_0	Permeability of vacuum	8
ρ	Gas density	15
χ	Susceptibility	6
$\chi^{(1)}$	First order component of susceptibility	6
$\chi^{(2)}$	Second order component of susceptibility	6
$\chi^{(3)}$	Third order component of susceptibility	6
ω_{AS}	Anti-Stokes frequency	6
ω_p	Pump frequency	4
ω_s	Stokes frequency	4
ω_v	Transition frequency	4

Abstract

High resolution cw coherent anti-Stokes Raman spectroscopy (CARS) was performed in molecular deuterium gas. Single mode argon ion and ring dye lasers were used to make accurate measurements of the Raman linewidths of the Q(0) through Q(4) transitions. These lines were examined at room temperature at pressures ranging from 0.35 to 20 atmospheres. The pressure broadening coefficient and the self diffusion coefficient of each line were obtained in this study and compared with other work. Additionally, the transition frequency of each line was measured and the frequency shift coefficients were obtained.

HIGH RESOLUTION COHERENT ANTI-STOKES RAMAN SPECTROSCOPY OF DEUTERIUM GAS

I. Introduction

Coherent anti-Stokes Raman spectroscopy (CARS) is a third order nonlinear optical mixing process primarily used to probe gases. Two laser beams interact with the medium being studied producing a weak, third beam with a higher frequency than either of the lasers. This laser spectroscopy technique was first discovered in the early 1960's, but it was not widely used until the mid 1970's.¹ With the development of high power tunable lasers, CARS has become a respected and reliable diagnostic tool.²

CARS can be used to nonintrusively determine the temperature or major species concentration of a gas.¹ Since it is an optical method, it can be used to study a flowing gas without disturbing the flow. It can also determine the temperature in an environment where a physical probe would be destroyed.

Several varieties of CARS systems exist to serve different purposes. Broadband CARS can produce an entire anti-Stokes spectrum during a single laser pulse, providing excellent temporal resolution. With this arrangement, the

medium and its spectrum may be studied in a dynamic system.³ High spectral resolution CARS is used on static systems to obtain detailed spectroscopic information, such as the linewidth and the center frequency of the transitions.⁴ Since this system may take several minutes to scan across one transition, the temporal resolution is poor, but the spectral resolution is much better than the broadband CARS. Either of these methods may be used to provide excellent spatial resolution by tightly focussing the beams to examine a small volume in the medium.⁵

In this experiment, molecular deuterium was studied to obtain some basic information. Pressure broadening and frequency shift coefficients were determined, which will aid in diagnostic work. Also, the system was improved to provide better data. The deuterium transitions were more difficult to obtain than the already observed hydrogen transitions because the signal was less intense. Improving the system will help the follow-on studies of hydrogen fluoride and deuterium fluoride, which are important lasing media.

This experiment, which employs a high spectral resolution cw CARS system, was designed to study all observable Q-branch transitions in deuterium over the largest available pressure range. Linewidth and transition frequency data were collected for the Q(0) through Q(4) transitions, while the pressure was varied from the lowest

pressure where the transitions are observable (0.35 atmospheres) to the highest available pressure (20 atmospheres).

Chapter II provides the necessary theory and background information to understand the experiment. Chapter III describes the experimental equipment, while Chapter IV explains the procedures that were used in this project. The experiment's results are reported in Chapter V. Chapter VI analyzes the data, extracts some coefficients, and compares these values with other reported work. Finally, some conclusions are drawn and recommendations are made in Chapter VII.

II. Theory

Coherent anti-Stokes Raman spectroscopy is based on the Raman effect, which was first observed by C. V. Raman.⁶ To understand this, Rayleigh scattering must first be discussed. When a photon and an atom or molecule collide, the particle gains the energy of the photon and then reemits a photon to reduce the energy of the particle. The energy of the absorbed photon and the energy of the emitted photon are usually the same, which is Rayleigh scattering. When the two photon energies are different, the result is the Raman effect. George Stokes extensively studied the situation where the emitted photon has less energy than the absorbed photon, commonly known as a Stokes transition.⁶ Stokes predicted that the emitted photon could never have more energy than the absorbed photon. However, this situation was observed and was given the name of an anti-Stokes (AS) transition.⁷

CARS is based on this type of interaction between photons and particles. As diagrammed in Figure 1, one photon, called a pump photon with a frequency of ω_p , interacts with the molecule to raise its energy to some virtual state. The molecule then releases energy and falls to an excited state through the stimulated emission of a Stokes photon, having a frequency of ω_s . The frequency difference between this excited state and the ground state is defined as the transition frequency, ω_v . The molecule is

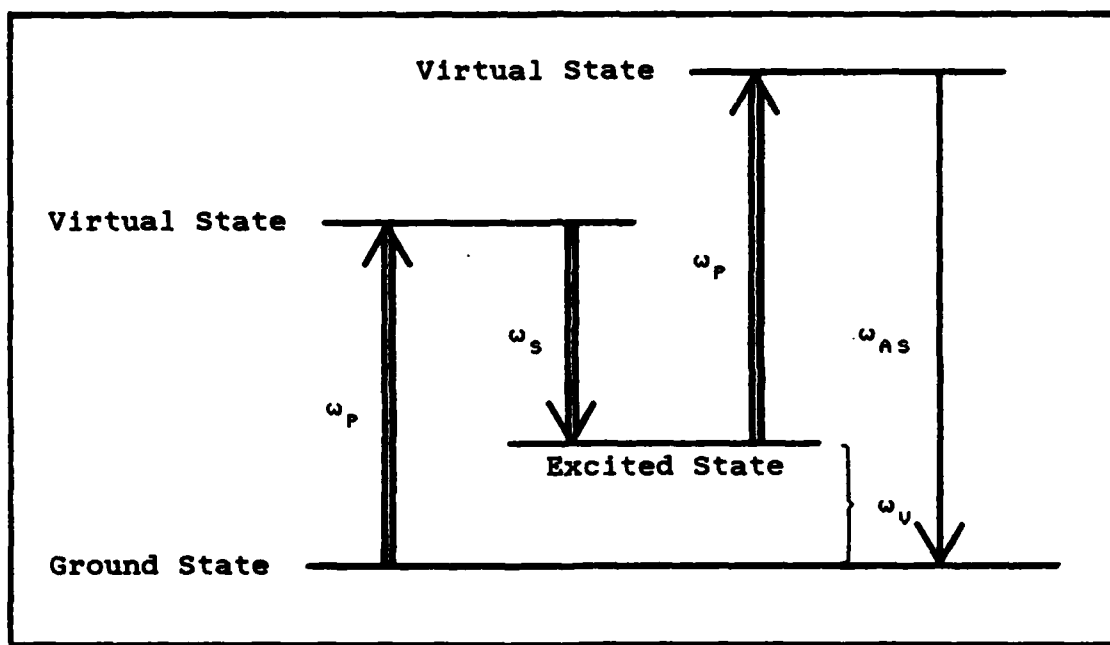


Figure 1. The CARS Process

then excited to another virtual state by another pump photon also of frequency ω_p . Finally, the molecule returns to its original state through the emission of an anti-Stokes photon with a frequency of ω_{AS} .

This operation requires the interaction of three photons to produce the desired AS photon and, therefore, is a third order nonlinear effect. Adequate understanding of this subject requires a discussion of nonlinear polarization, as well as the generation of the AS wave from the wave equation. The nonlinear susceptibility, based on the simple harmonic oscillator and resonance, will then be developed. Finally, the expected linewidths will be discussed and the deuterium transition frequencies will be derived.

Nonlinear Polarization

Induced polarization is the response of a dielectric medium to an applied electromagnetic field. While polarization is commonly considered a linear response to the field, there are higher order nonlinear terms, also. Therefore, the polarization may be expanded as

$$P = \epsilon_0 \chi E \quad (1a)$$

$$= \epsilon_0 [\chi^{(1)} + \chi^{(2)}E + \chi^{(3)}EE + \dots] E \quad (1b)$$

$$= \epsilon_0 \chi^{(1)}E + \epsilon_0 [\chi^{(2)}E + \chi^{(3)}EE + \dots] E \quad (1c)$$

$$= P^{(L)} + P^{(NL)} \quad (1d)$$

where P = polarization
 ϵ_0 = permittivity in a vacuum
 χ = susceptibility
 E = electric field intensity
 $\chi^{(1)}$ = linear component of susceptibility
 $\chi^{(2)}$ = quadratic component of susceptibility
 $\chi^{(3)}$ = cubic component of susceptibility
 $P^{(L)}$ = linear component of polarization
 $P^{(NL)}$ = nonlinear component of polarization

In CARS, the electric field is the sum of the fields from the pump and Stokes fields, which are provided by lasers. Therefore, if the lasers are propagating in the z direction,

$$E = E_p + E_s \quad (2a)$$

$$= A_p e^{i[k_p z - \omega_p t]} + A_s e^{i[k_s z - \omega_s t]} + c.c \quad (2b)$$

where A = amplitude of the field
 k = propagation vector
 c.c. = complex conjugate of all preceding terms

Since we have already seen that the CARS process is a function of three photons, then the process must be a third order effect, requiring concentration on the third order polarization, $P^{(3)}$, where

$$P^{(3)} = \epsilon_0 \chi^{(3)} E E E \quad (3a)$$

$$\begin{aligned} = \epsilon_0 \chi^{(3)} & \left[A_p^3 e^{3P} + 3|A_p|^2 A_p e^P + 6|A_p|^2 A_s e^S \right. \\ & + 3A_p^2 A_s e^{2P+S} + 3A_p^2 A_s^* e^{2P-S} + 3A_p A_s^{*2} e^{P-2S} \\ & + 3A_p A_s^2 e^{P+2S} + 6|A_s|^2 A_p e^P + 3|A_s|^2 A_s e^S \\ & \left. + A_s^3 e^{3S} + c.c. \right] \quad (3b) \end{aligned}$$

where A^* is the complex conjugate of A , and in the exponents $P = i[k_p z - \omega_p t]$ and $S = i[k_s z - \omega_s t]$. The CARS process is specifically concerned with the situation where two pump photons are absorbed and one Stokes photon is emitted. In terms of frequency, this combination is $2\omega_p - \omega_s$. Thus, the CARS polarization is

$$P_{CARS} = 3 \epsilon_0 \chi^{(3)} A_p^2 A_s^* e^{2P-S} + c.c. \quad (4)$$

Generation of the Anti-Stokes Wave

The polarization that was just developed will be used in this section to generate the AS wave. The wave equation describing the propagation of an electromagnetic field in a lossless, nonmagnetic medium is

$$\nabla^2 E = \mu_0 \epsilon_0 \frac{\partial^2 E}{\partial t^2} + \mu_0 \frac{\partial^2 P}{\partial t^2} \quad (5)$$

The expression for polarization in equation (1b) can be substituted into (5) yielding

$$\nabla^2 E = \mu_0 \epsilon_0 \frac{\partial^2}{\partial t^2} E + \mu_0 \epsilon_0 \frac{\partial^2}{\partial t^2} [\chi^{(1)} + \chi^{(2)} E + \chi^{(3)} EE + \dots] E \quad (6a)$$

$$= \frac{n^2}{c^2} \frac{\partial^2}{\partial t^2} E + \mu_0 \epsilon_0 \frac{\partial^2}{\partial t^2} [\chi^{(2)} E + \chi^{(3)} EE + \dots] \quad (6b)$$

where $n^2 = 1 + \chi^{(1)}$ and $c^2 = 1/(\mu_0 \epsilon_0)$.

CARS is commonly used to study gases, which are all isotropic. Inversion symmetry is a characteristic of all isotropic materials, which means all even order susceptibilities are zero.⁸ If $\chi^{(5)}$ and all other odd higher order susceptibilities are assumed negligible, then the infinite series in equation (6b) becomes

$$\nabla^2 E - \frac{n^2}{c^2} \frac{\partial^2}{\partial t^2} E = \mu_0 \epsilon_0 \frac{\partial^2}{\partial t^2} \chi^{(3)} EEE \quad (7a)$$

$$= \mu_0 \frac{\partial^2}{\partial t^2} P_{\text{CARS}} \quad (7b)$$

To solve this equation, a steady state solution of $E(t) = A_{\Lambda s}(z) e^{\Lambda s}$ is assumed, where $A_{\Lambda s}(z)$ is the spatially varying amplitude and $e^{\Lambda s}$ represents $\exp i[k_{\Lambda s} z - \omega_{\Lambda s} t]$, similar to e^p and e^s . When the spatial derivatives are completed,

$$\nabla^2 E = \frac{\partial^2 A_{\Lambda s}}{\partial z^2} e^{\Lambda s} + 12k_{\Lambda s} \frac{\partial A_{\Lambda s}}{\partial z} e^{\Lambda s} - k_{\Lambda s}^2 A_{\Lambda s} e^{\Lambda s} \quad (8a)$$

$$= 12k_{\Lambda s} \frac{\partial A_{\Lambda s}}{\partial z} e^{\Lambda s} - k_{\Lambda s}^2 A_{\Lambda s} e^{\Lambda s} \quad (8b)$$

The last equality assumed a slowly varying amplitude such

that $\frac{\partial^2 A_{\Lambda s}}{\partial z^2} \ll k_{\Lambda s} \frac{\partial A_{\Lambda s}}{\partial z}$. The time derivative is

$$\frac{n^2}{c^2} \frac{\partial^2 E}{\partial t^2} = - \left[\frac{n\omega_{\Lambda s}}{c} \right]^2 A_{\Lambda s} e^{\Lambda s} \quad (9a)$$

$$= -(k_{\Lambda s})^2 A_{\Lambda s} e^{\Lambda s} \quad (9b)$$

Inserting these last two results into equation (7b) yields

$$12k_{\Lambda s} \frac{\partial A_{\Lambda s}}{\partial z} e^{\Lambda s} = \mu_0 \frac{\partial^2}{\partial t^2} P_{CARS} \quad (10)$$

The CARS polarization from equation (4) can be substituted here and the equation can be integrated to find the AS amplitude. If the pump field is assumed to lose no power in the interaction, the result is

$$A_{\Lambda s} = \frac{13\omega_{\Lambda s}}{2cn} \chi^{(3)} A_p^2 A_s^* z \exp\left[\frac{i\Delta kz}{2}\right] \text{sinc}\left[\frac{\Delta kz}{2}\right] \quad (11)$$

where $\text{sinc}[x] = (\sin x)/x$ and $\Delta k = 2k_p - k_s - k_{\Lambda s}$.

To obtain phase match, Δk must equal zero.

To find the power of the AS beam, this amplitude is squared and scaled by the focal volume where the photon-particle interaction takes place. Also, the fields are assumed to be Gaussian beams, which is a good approximation for the lasers. When this is done,

$$P_{As} = C \left[\frac{4\pi\omega_p \omega_{As}}{c} \right]^2 |\chi^{(3)}|^2 P_p^2 P_s \quad (12)$$

where P = power (not polarization)

c = speed of light in a vacuum

C = constant that depends on the definition of the

focal volume and varies by authors.^{2,8,10,11}

The primary point of this section is that the anti-Stokes power is proportional to the square of the third order susceptibility.

Susceptibility

The significance of the power being proportional to the square of $\chi^{(3)}$ can be understood by classically studying the susceptibility, based on the theory by Placzek, as presented by Roh.² Thus far, the polarization has been viewed on a macroscopic scale. Now the molecules will each be considered as simple harmonic oscillators. Each of the N molecules will have an induced molecular polarizability, $\alpha(t)$, which can be expanded by a Taylor series about the internuclear spacing $q(t)$. Therefore, the polarization becomes

$$P = N \alpha(t) E \quad (13a)$$

$$= N \left[\alpha_0 + \left. \frac{\partial \alpha}{\partial q} \right|_{q_0} q(t) \right] E \quad (13b)$$

The electric field, E , is the sum of the pump and Stokes fields as in equation (2b).

More terms must be defined to proceed towards the equation of motion of a molecule. The interaction energy, H , between an electromagnetic field and a molecular media is

$$H = \frac{-1}{2} P E \quad (14a)$$

$$= \frac{-1}{2} N \left[\alpha_0 + \frac{\partial \alpha}{\partial t} \bigg|_{q_0} q(t) \right] E E \quad (14b)$$

The nonlinear polarization is defined as

$$P^{(NL)} = - \frac{\partial H}{\partial E} = N \frac{\partial \alpha}{\partial q} \bigg|_{q_0} q(t) E \quad (15)$$

The molecular driving force is

$$F = \frac{-1}{N} \frac{\partial H}{\partial q} = \frac{1}{2} \frac{\partial \alpha}{\partial q} \bigg|_{q_0} E E \quad (16)$$

Now the equation of motion may be written as

$$\frac{\partial^2 q}{\partial t^2} + \Gamma \frac{\partial q}{\partial t} + \omega_v^2 q = \frac{F}{m} = \frac{1}{2m} \frac{\partial \alpha}{\partial q} \bigg|_{q_0} E E \quad (17)$$

where Γ = damping coefficient

ω_v = resonant frequency

m = reduced mass of molecule

A solution of the form

$$q = Q e^{i\omega t} + c.c. \quad (18)$$

is assumed, where Q is the amplitude and the exponent means the same as before. This gives a solution of

$$q = \frac{1}{m} \frac{\partial \alpha}{\partial q} \bigg|_{q_0} \frac{A_p A_s^*}{\omega_v^2 - (\omega_p - \omega_s)^2 - i(\omega_p - \omega_s)\Gamma} e^{p-s} + \text{c.c.} \quad (19)$$

By substituting this result into the equation for nonlinear polarization, equation (15),

$$P^{(NL)} = \frac{N}{m} \left[\frac{\partial \alpha}{\partial q} \bigg|_{q_0} \right]^2 \frac{A_p A_s^*}{\omega_v^2 - (\omega_p - \omega_s)^2 - i(\omega_p - \omega_s)\Gamma} e^{2p-s} \quad (20)$$

$$= 3\epsilon_0 \chi^{(3)} A_p^2 A_s^* e^{2p-s} \quad (4)$$

The second equality is equation (4). Equating the right hand sides of equation (20) and equation (4) produces an expression for $\chi^{(3)}$.

$$\chi^{(3)} = \frac{N}{3\epsilon_0 m} \left[\frac{\partial \alpha}{\partial q} \bigg|_{q_0} \right]^2 \frac{1}{\omega_v^2 - (\omega_p - \omega_s)^2 - i(\omega_p - \omega_s)\Gamma} \quad (21)$$

The Raman scattering coefficient $\frac{\partial \sigma}{\partial \Omega}$ is related to $\frac{\partial \alpha}{\partial q}$ by¹²

$$\frac{\partial \sigma}{\partial \Omega} = \frac{h \omega_s^4}{4\pi m \omega_v c^4} \left[\frac{\partial \alpha}{\partial q} \bigg|_{q_0} \right]^2 \quad (22)$$

When (22) is inserted into (21), the result is

$$\chi^{(3)} = \frac{4\pi N c^4}{3\epsilon_0 h \omega_s^4} \left[\frac{\partial \sigma}{\partial \Omega} \right] \frac{\omega_v}{\omega_v^2 - (\omega_p - \omega_s)^2 - i(\omega_p - \omega_s)\Gamma} \quad (23)$$

Using the simple harmonic oscillator model, Γ can be viewed as the damping coefficient. Optically, Γ represents the linewidth of a given transition. When the system is at resonance, with the pump and Stokes frequencies separated by the transition frequency, ω_v , the portion of equation (23)

after the cross section will change to $\frac{1}{\Gamma}$, so that the susceptibility is inversely proportional to the linewidth. From equation (12), the power of the AS beam is proportional to the square of $\chi^{(3)}$ which leads to

$$P_{AS} \sim \left[\frac{1}{\Gamma} \right]^2 \quad (24)$$

This relationship between linewidth and power is the important result. If the linewidth is known, then predictions can be made about the AS power.

Linewidth Dependence on Pressure

The transition linewidth, which is important to CARS, is dependent on pressure in a number of ways. In the low pressure range below a few tenths of an atmosphere, the transition is Doppler broadened by the thermal motion of the molecules. Above a few atmospheres, pressure broadening dominates the linewidth due to the increased number of collisions.

Between these two pressure regions, the pressure of the gas compresses the molecules so that they cannot attain as great a speed, and thus, the Doppler broadened linewidth decreases. However, the pressure is not high enough for the collisions to dominate the linewidth through pressure broadening. In this region, the two broadening forces work together to produce a narrower line. This phenomenon is known as Dicke narrowing.¹³

Dicke's model of this narrowing and the pressure broadening model are combined to describe the linewidth in the region of interest to give

$$\Delta\nu = \frac{4\pi D_0}{\lambda^2 c \rho} + a\rho \quad (25)$$

where $\Delta\nu$ = the full width half maximum (FWHM) linewidth

D_0 = the self-diffusion coefficient

λ = the wavelength of the transition

ρ = the density of the gas

a = the pressure broadening coefficient

This experiment will determine D_0 and a .

Transition Frequencies

The transitions to be studied in this experiment are the Q-branch transitions. This implies that the transition will be from the ground vibrational state to one vibrational state above the ground state. Using the vibrational quantum number, v , the transition will be between $v = 0$ and $v = 1$. Throughout all this, the rotational quantum number, J , will not change. Therefore, $Q(J)$ will represent a change in the vibrational state, but the rotational state will remain J . For example, $Q(2)$ represents the transition between the $v = 0$, $J = 2$ state and the $v = 1$, $J = 2$ state.

The transition frequencies can be calculated from the Dunham coefficients. The energy of a given level (in units

of cm^{-1}) may be calculated from¹⁴

$$\begin{aligned} E(v, J) = & \omega_e(v+.5) - \omega_e x_e(v+.5)^2 + \omega_e y_e(v+.5)^3 \\ & + \omega_e z_e(v+.5)^4 + [B_e - \alpha_e(v+.5)] J(J+1) \\ & - [D_e + \beta_e(v+.5)] J^2(J+1)^2 \end{aligned} \quad (26)$$

where E is the energy of the level, v and J are quantum numbers, and all other variables are Dunham coefficients. The difference in energy between any two levels is used to calculate the transition frequency.

The units of reciprocal centimeters, cm^{-1} , are really the units for wavenumbers. The wavenumber is simply the inverse of the wavelength in vacuum in units of centimeters. The conversion between Hertz and reciprocal centimeters is $30\text{MHz} = 1\text{cm}^{-1}$. Energy may be derived by multiplying the frequency in Hertz by Planck's constant. In this paper, the term "frequency" will describe numbers with units of Hertz or cm^{-1} , while the term "wavenumber" will strictly apply to numbers with the units of cm^{-1} .

The Dunham coefficients for deuterium, given in Reference 14 and shown in Table I, were used to calculate the Q-branch transition frequencies shown in Table II. These transition frequencies were then used to calculate the Stokes and AS frequencies, based on the pump frequency.

TABLE I
Dunham Coefficients for Deuterium
(From Reference 14)

ω_e	= 3115.50	B_e	= 30.4436
$\omega_e x_e$	= 61.82	α_e	= 1.0786
$\omega_e y_e$	= 0.562	D_e	= 0.0141
$\omega_e z_e$	= -0.0228	β_e	= -0.000224

TABLE II
Deuterium Transition Frequencies

Transition	Frequency (cm^{-1})
Q(0)	2993.801
Q(1)	2991.691
Q(2)	2987.476
Q(3)	2981.167
Q(4)	2972.779
Q(5)	2962.337

III. Experimental Equipment

Four types of equipment were used in this experiment. Lasers provided the Stokes and pump beams. Diagnostic equipment was used to determine the frequencies of the lasers and to detect problems with the lasers, such as mode hopping. A gas handling system was used to control the pressure in the sample cell where the anti-Stokes beam was generated. The last type of equipment detected the anti-Stokes beam and records its linewidth and frequency. Figure 2 is a block diagram of the equipment used in this experiment. The numbers in the figure also appear in parenthesis in this chapter when the equipment is discussed.

Lasers

Two laser systems were used to provide the pump and Stokes beams, which generate the anti-Stokes beam. A cw Spectra-Physics Model 165 argon ion laser(1) produced the 500mW single mode pump beam. Using an intracavity etalon, the laser was tuned to one of the iodine absorption lines near the center of the 514.5nm gain curve. While the wavenumber of this line is not recorded in the iodine atlas;¹⁵ it was estimated to be 19429.73cm^{-1} by interpolation. An iodine cell(2) was inserted in the pump beam between scans to monitor the frequency of the laser. The fluorescence, which was detected by a photomultiplier tube(3), was maximized to ensure the laser was operating near the peak of

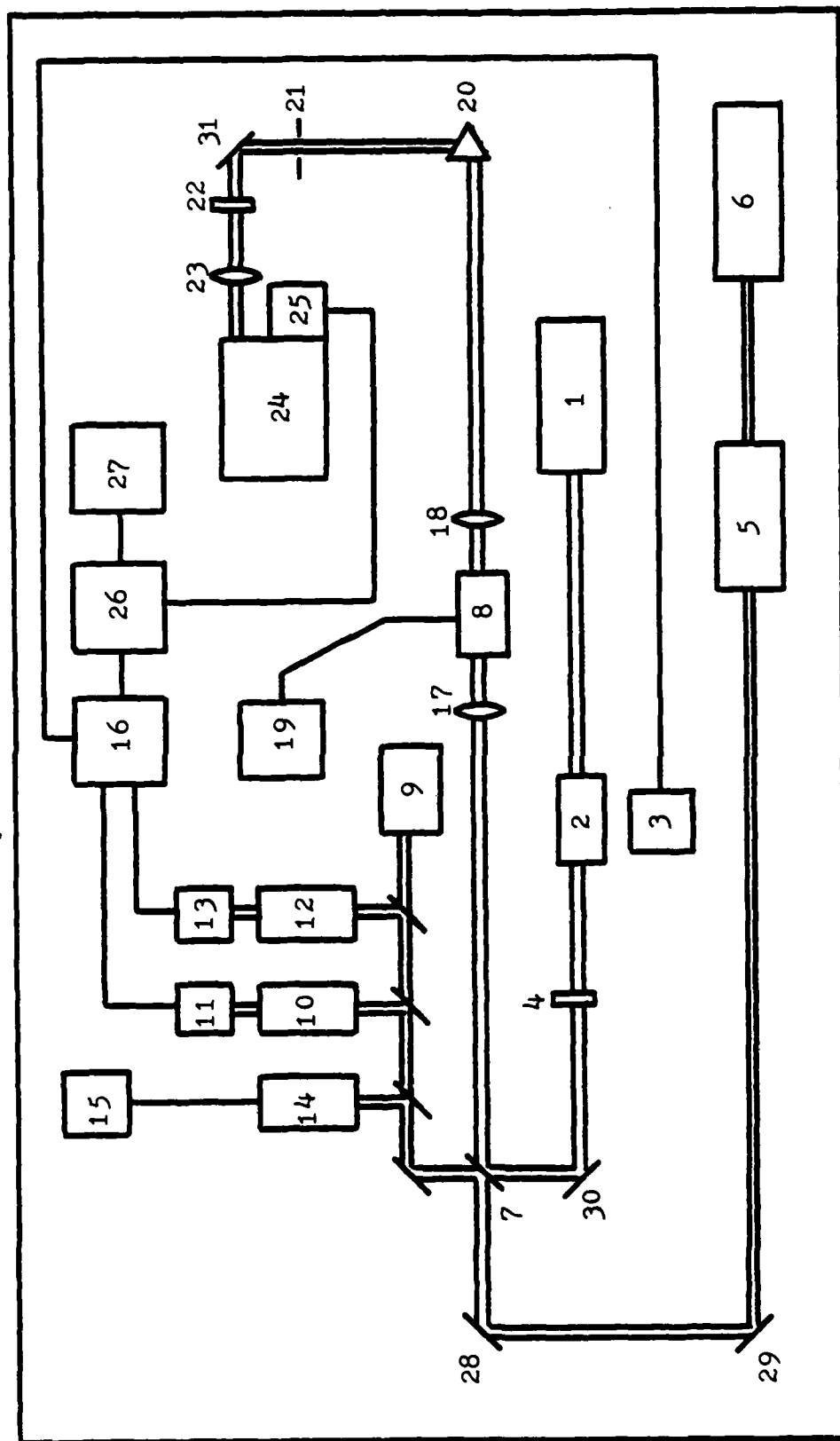


Figure 2. Block Diagram of the CARS System. The components are: argon ion lasers 1,6; iodine cells 2,10; photomultiplier tubes 3,25; filters 4,22; dye laser 5; dichroic mirror 7; sample cell 8; wavemeter 9; photodiodes 11,13; semi-confocal Fabry-Perot 12; spectrum analyzer 14; oscilloscope 15; chart recorder 16; lenses 17,18,23; gas handling system 19; prism 20; aperture 21; monochromator 24; discriminator 26; photon counter 27; mirrors 28,29,30,31.

that absorption line. During each scan, the stability of the laser was monitored by the diagnostic equipment described later. A long pass 470nm cut on filter(4) was placed in the pump beam to attenuate the emission from the plasma tube in the laser. Without this filter, the plasma tube emission overwhelmed the AS signal.

The cw Stokes beam was produced by a Coherent 699-21 tunable dye laser(5) with approximately 200 mW of power and a linewidth of 1MHz. Frequency stability was maintained with a servo control loop which minimized mode hopping. The stability of this laser was also monitored with the diagnostic equipment. The Rhodamin 6G dye used in the dye laser was pumped by a Spectra-Physics Model 171 argon ion laser(6) operating at 514.5nm between 6 and 7 watts.

A dichroic mirror(7) was used to collinearly combine the pump and Stokes beams, directing the majority of the power from each beam into the sample cell(8). A small portion of each beam's power was diverted by the dichroic mirror(7) to the diagnostic equipment.

Diagnostic Equipment

A variety of equipment was used to determine the frequency and monitor the stability of each beam. The diagnostics also provided a relative frequency marker to determine the linewidth of the anti-Stokes transition.

A Burleigh Model WA-10 Wavemeter(9) was used to determine the approximate frequency of the dye laser. While

the wavemeter was not accurate enough to provide the absolute frequency, it did give a real time frequency measurement within about 0.02 cm^{-1} , which was very helpful in tuning the dye laser.

An iodine absorption cell(10) was used to determine the exact frequency of the dye laser. The dye laser was scanned across a range that contained at least two prominent iodine absorption peaks near the Stokes frequency. The wavemeter displayed the approximate frequency of the absorption lines. Comparison of the observed absorption with an atlas¹⁵ of iodine lines firmly established the absolute frequency. A PIN photodiode(11) was used to detect the throughput power.

A semi-confocal Fabry-Perot cavity(12) was used to establish a relative frequency mark to measure the anti-Stokes linewidth. The free spectral range of the Fabry-Perot was calculated to 124 MHz (0.00413 cm^{-1}) by scanning the dye laser over a large range and counting Fabry-Perot resonant peaks between two iodine absorption lines. A PIN photodiode(13) was used to detect the resonant peaks from the Fabry-Perot cavity.

To monitor the stability of the pump and Stokes beams, a scanning Fabry-Perot spectrum analyzer(14) was used. The frequency and amplitude stability could be determined by watching the oscilloscope(15) that displayed the spectrum analyzer output. Amplitude stability was monitored by observing the height of the peaks on the scope, while

frequency stability was determined by the lateral position of the spikes. This made mode hopping and multi-mode operation easy to detect.

Finally, a dual channel strip chart recorder(16) recorded the response of the detectors behind the absorption cell and the semiconfocal cavity, as well as the response of the detection system.

Gas Handling System

The majority of the Stokes and pump beams from the dichroic mirror(7) were focussed into the gas sample cell(8) by a lens(17) with a 10 cm focal length. Here they interacted with the deuterium and generated the anti-Stokes beam. Upon exiting the sample cell, the three collinear beams were gently focussed into the detection system by a 15cm focal length lens(18). The pressure within the sample cell was regulated by a gas handling system(19). The system was designed and constructed during this project to control the pressure from a few torr to several hundred psi.

Detection Equipment

The three beams from the sample cell were focussed into the detection system, which counted the anti-Stokes photons. First, the AS beam was spatially separated from the other beams by a Pellin-Broca prism(20). The pump and Stokes beams were stopped by an aperture(21) through which only the AS beam was allowed to pass. The various frequencies of the

different transitions were passed by rotating the prism which was mounted on a micrometer driven turntable. To filter out any scattered light, the light passing through the aperture hit a 9.0nm bandpass interference filter(22) which was angle tuned to the AS frequency.

The light passing the interference filter, primarily the AS signal, was focussed by a 284mm lens(23) onto the entrance slit of a Jarrel-Ash monochromator(24) which was set at the AS wavelength. An RCA 8850 photomultiplier tube(25), operated at 1200V, was mounted on the exit slit of the monochromator. The photomultiplier was thermo-electrically cooled, which reduced the typical dark count to 30 counts per second and thus increased the signal-to-noise ratio.

The output of the photomultiplier entered a photon counting system including an EG&G Model 1121 Amplifier/Discriminator(26) and an EG&G Model 1112 Photon Counter/Processor(27). The discriminator was set to eliminate the majority of the non-photon noise. The output of the discriminator entered the photon counter which digitally displayed the photon count per second. The discriminator also delivered an analog signal to the strip chart recorder(16) which displayed the count rate of the AS photons along with the output of one of the pieces of diagnostic equipment.

IV. Procedures

The procedure followed in this experiment was conceptually simple, but complicated to implement. Conceptually, the dye laser had to be tuned to a Stokes frequency and scanned across a range centered about that frequency. To find the frequency of the transition, the AS line had to be recorded on the strip chart recorder along with at least two prominent iodine absorption peaks. Measuring the distance from the iodine peaks to the AS peak determined the Stokes frequency and, in turn, the transition frequency. To find the linewidth of the AS line, the resonant peaks from the semi-confocal Fabry-Perot were recorded along with the AS line. Counting resonant peaks within the FWHM of the AS line determined the width of the AS line.

Experimental Procedure

Implementing this concept was complicated and just finding an AS line was tedious. To do that, the pump beam frequency had to be established first. This was accomplished by placing an iodine cell in the beam and detecting the fluorescence of the iodine line near the center of the Ar^+ 514.5nm gain curve. The pump laser intracavity etalon was adjusted to maximize the single mode output while also maximizing the iodine fluorescence. Single mode operation could be determined by observing the

mode structure displayed on the oscilloscope connected to the spectrum analyzer. After adjusting the etalon, the laser stabilized in a few minutes and usually did not need adjustment for the rest of the day.

Before finding the AS line, all the optics had to be adjusted. The overlap of the beams was set by moving the mirrors(7,28,29,30 in Figure 2) and observing the overlap on the lenses near the sample cell. The detection system was tuned by setting the monochromator to the AS wavelength, removing the long pass filter from the pump beam, and optimizing all the detection equipment to maximize the detected emission from the argon laser plasma tube. This included rotating the Pellin-Broca prism(20 in Figure 2), moving the mirror(31), rotating the interference filter(22) and adjusting the lens(23) near the entrance slit of the monochromator.

To find the AS line, the sample cell was filled to the appropriate pressure, the long pass filter was placed in the pump beam, and the dye laser was scanned across a frequency range that included the Stokes frequency, as calculated from the Dunham coefficients. Once the line was found, the dye laser was kept on the Stokes frequency and the AS signal was optimized by improving the overlap and the detection equipment alignment. Late in the study, it was discovered that if the overlap and detection adjustments were iteratively optimized, the maximum photon count could be significantly improved. Watching the strip chart recorder,

instead of the digital display on the photon counter, made it easier to establish trends which helped maximize the signal count.

Once all the optics were optimized, the dye laser had to be adjusted to properly scan across the desired frequencies. Since the iodine peaks were often widely spaced, the dye laser cavity mirrors and the internal thin etalon had to be carefully set so that the laser would make a complete scan without mode hopping.

With everything set, the frequency of the argon laser was once again checked with the iodine cell. Then, the iodine cell was removed to maximize the pump power delivered to the sample cell. Three good scans were then made to determine the frequency or linewidth of the AS line. A good scan meant the baselines on each side of the iodine peaks, as well as the AS peak, were visible. Also, the lines could not be distorted nor could mode hopping occur.

To record the frequency of the AS line, the iodine cell throughput PIN detector and the photon counting system were connected to the strip chart recorder. The dye laser was operated for three good scans, each including at least two prominent iodine absorption peaks that were physically near the AS peak on the chart paper. After the three scans, the frequency of the pump laser was again checked with the iodine cell.

To record the linewidth of the AS line, the PIN photodetector behind the semi-confocal Fabry-Perot was

connected to the chart recorder in place of the iodine cell detector. The dye laser scan width was reduced to make the AS wider on the chart paper allowing a more accurate measurement. With this arrangement, three more good scans were recorded with the AS peak and the semi-confocal Fabry-Perot resonant peaks.

This procedure was used for each observable transition for each pressure. The pressures studied were 0.35, 0.5, 0.7, 1.0, 1.5, 2.2, 3.5, 5.0, 7.0, 10, 15, and 20 atmospheres. These pressures were selected because, on a logarithmic scale, they uniformly covered the range of pressures from the lowest pressure where the lines were observable to the highest available pressure. The sample cell was at room temperature, which was usually 22°C.

Analytical Procedure

A graphical procedure was used to extract the data from the strip charts. The Stokes frequency was determined by comparing the center frequency of the AS line with the center frequencies of the iodine lines. The center of the FWHM width was used to mark the center of each line. This method was closest to marking the center of gravity, which the atlas¹⁵ used to determine the center frequency of the asymmetric iodine lines. This method also worked well for the AS line because sometimes the noise made it difficult to select a peak or the noise skewed the peak. One problem encountered was that the iodine peaks were absorption peaks

and not fluorescence peaks. The difference is that the baseline changed as the power of the dye laser changed across a scan. While this should not have affected the data, reading the data from the charts became more complicated.

To determine the Stokes frequency, the distance between iodine peaks was measured as well as the distance from one iodine peak to the AS peak. This last distance had to be adjusted by 4mm because the two pens on the chart recorder were separated by that distance. The ratio between the peaks, combined with the frequency difference between iodine peaks from the atlas^{15,16} allowed the Stokes frequency to be calculated. The transition frequency was then calculated by subtracting the Stokes frequency from the pump frequency.

The linewidth calculation was much easier. The FWHM of the AS line and the distance between a large number of semi-confocal Fabry-Perot peaks were measured from the chart paper. The ratio of these distances along with the number of peaks led to the number of peaks within the AS linewidth. This result was multiplied by the free spectral range of the semi-confocal Fabry-Perot to produce the AS linewidth.

V. Results

This project was designed to find all observable anti-Stokes transitions in D_2 between the lowest pressure where the lines were observable and the highest available pressure. The linewidth and frequency of these transitions were to be measured. The observable transitions were Q(0) through Q(4), with Q(1) and Q(2) clearly being the strongest transitions. A search was conducted for the Q(5) line, but it could not be found with this system.

For each transition, the pressure was decreased until the signal was no longer detectable. Table III shows the lowest pressure for each line that the signal could be observed. This table also indicates the relative strength of each transition with the stronger transitions being observable at lower pressures.

TABLE III
Lowest Pressure with an Observable AS Signal

Transition	Pressure
Q(0)	0.7 atm
Q(1)	0.5 atm
Q(2)	0.35 atm
Q(3)	0.7 atm
Q(4)	1.0 atm

The highest pressure available from the gas cylinder was 20 atmospheres. The linewidth measurements for the

three weaker lines, however, were not reliable beyond 10 atmospheres. In this high pressure range, the lines were too broad compared to their heights to make a valid linewidth measurement. The center frequency measurements were still valid though. For these measurements, the dye laser scanned across a broader frequency range, which means the time the dye laser was on the Stokes frequency was shorter. Consequently, the AS signal was present for a shorter time, so the AS line was compressed on the chart paper. The peak was then defined well enough to make the lines observable and provide reliable data.

The linewidth and frequency of the $Q(0)$ through $Q(4)$ transitions at each pressure are presented on the following pages in Tables IV through VIII, respectively. Some general trends can be seen that will become more obvious in the next chapter. The widths of the lines decrease as the pressure increases in the low pressure range. This is a manifestation of the Dicke narrowing. The linewidths reach a minimum near one atmosphere and start increasing as the pressure increases. This is due to pressure broadening. Also, the transition frequency tends to decrease as the pressure increases, which is a characteristic known as frequency shifting. The heights of the peaks are not reported as a function of pressure because too many variables are involved to provide any meaningful results. Some of these variables include output power of both lasers, the overlap alignment, and the detection equipment alignment. In view of this,

TABLE IV

Linewidth and Frequency of Q(0) Transition

Pressure (atm)	Linewidth (cm^{-1})	Frequency (cm^{-1})
0.7	0.0111	2993.6061
1.0	0.0092	2993.6047
1.5	0.0098	2993.6060
2.2	0.0133	2993.6060
3.5	0.0205	2993.6035
5.0	0.0279	2993.6023
7.0	0.0381	2993.6231
10.0	0.0541	2993.6074
15.0	-	2993.5843
20.0	-	2993.5828

TABLE V

Linewidth and Frequency of Q(1) Transition

Pressure (atm)	Linewidth (cm^{-1})	Frequency (cm^{-1})
0.5	0.0082	2991.5227
0.7	0.0070	2991.5228
1.0	0.0058	2991.5197
1.5	0.0064	2991.5028
2.2	0.0075	2991.5037
3.5	0.0085	2991.5024
5.0	0.0116	2991.5110
7.0	0.0181	2991.5128
10.0	0.0268	2991.4992
15.0	0.0383	2991.4740
20.0	0.0468	2991.4787

TABLE VI

Linewidth and Frequency of Q(2) Transition

Pressure (atm)	Linewidth (cm^{-1})	Frequency (cm^{-1})
0.35	0.0108	2987.2905
0.5	0.0089	2987.2871
0.7	0.0084	2987.2847
1.0	0.0081	2987.2942
1.5	0.0086	2987.3011
2.2	0.0100	2987.3008
3.5	0.0142	2987.2993
5.0	0.0188	2987.2946
7.0	0.0291	2987.2911
10.0	0.0363	2987.2711
15.0	0.0548	2987.2547
20.0	0.0712	2987.2529

TABLE VII

Linewidth and Frequency of Q(3) Transition

Pressure (atm)	Linewidth (cm^{-1})	Frequency (cm^{-1})
0.7	0.0082	2980.9937
1.0	0.0083	2981.0052
1.5	0.0089	2981.0019
2.2	0.0123	2980.9991
3.5	0.0162	2980.9921
5.0	0.0203	2980.9970
7.0	0.0260	2980.9645
10.0	0.0381	2980.9873
15.0	-	2980.9583
20.0	-	2980.9552

TABLE VIII

Linewidth and Frequency of Q(4) Transition

Pressure (atm)	Linewidth (cm ⁻¹)	Frequency (cm ⁻¹)
1.0	0.0073	2972.6294
1.5	0.0079	2972.6274
2.2	0.0098	2972.6267
3.5	0.0136	2972.6228
5.0	0.0181	2972.6193
7.0	0.0241	2972.6086
10.0	0.0374	2972.6169
15.0	-	2972.5903
20.0	-	2972.5847

some common photon counts per second for each AS peak are shown in Table IX just to provide another indication of the strength of each transition.

Sample strip chart recordings for each type of measurement are provided in Figures 3 and 4 to show the signal-to-noise ratio. Figure 3 is a sample linewidth measurement. The lower trace is the AS photon count as determined by the photon counting equipment, while the upper trace shows the semi-confocal Fabry-Perot peaks. On the original chart paper, the resonant peaks are all the same shape and they are all equally spaced, indicating that the dye laser was stable throughout the scan. A sample of the frequency measurement is shown in Figure 4, with the lower trace again being the detected AS signal. This time, the upper trace shows the iodine absorption lines that the dye laser passed through during its scan.

TABLE IX

Usual Maximum Photon Counts	
Transition	Count per second
Q(0)	500
Q(1)	1200
Q(2)	2000
Q(3)	400
Q(4)	250

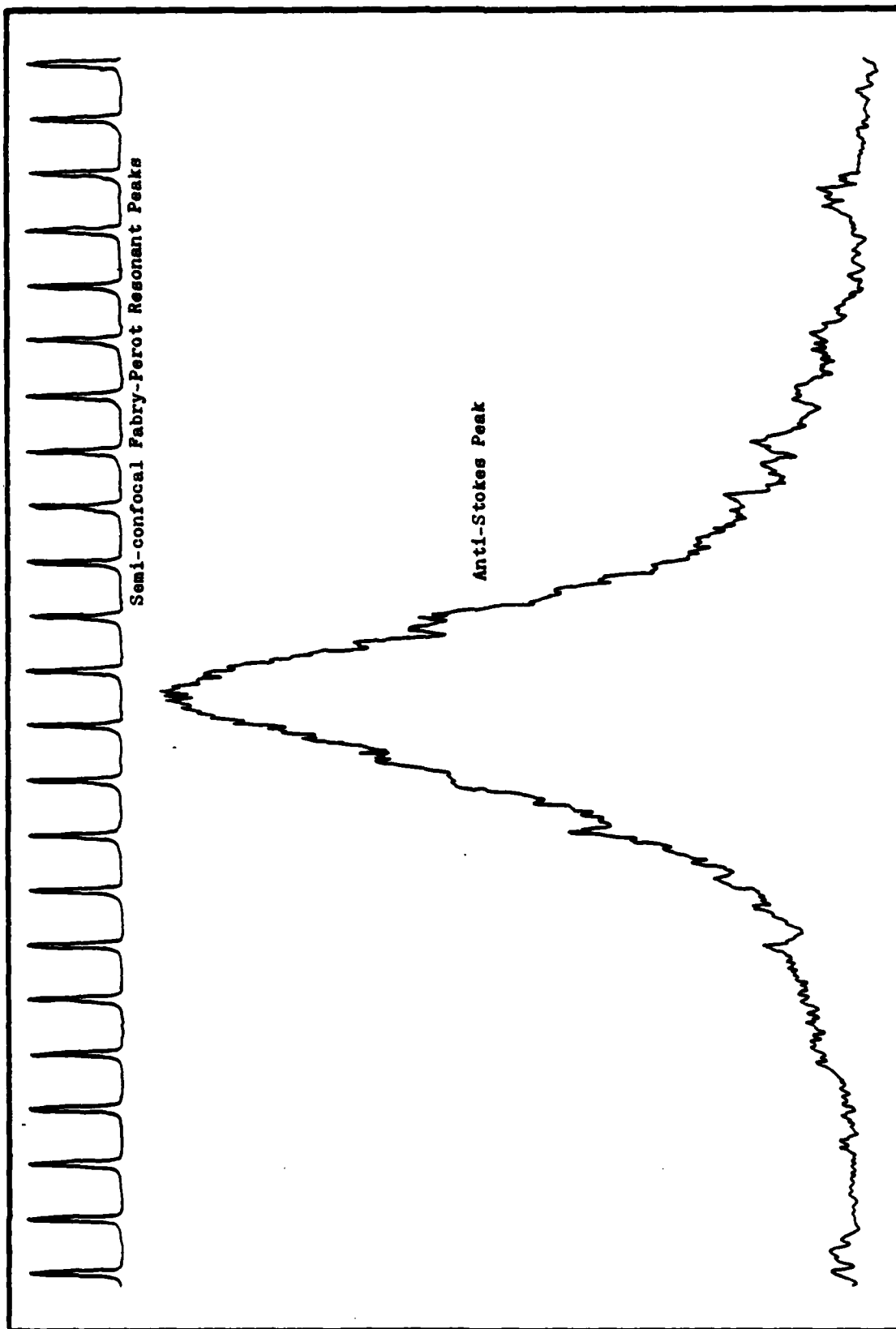


Figure 3. Sample Linewidth Strip Chart Recording

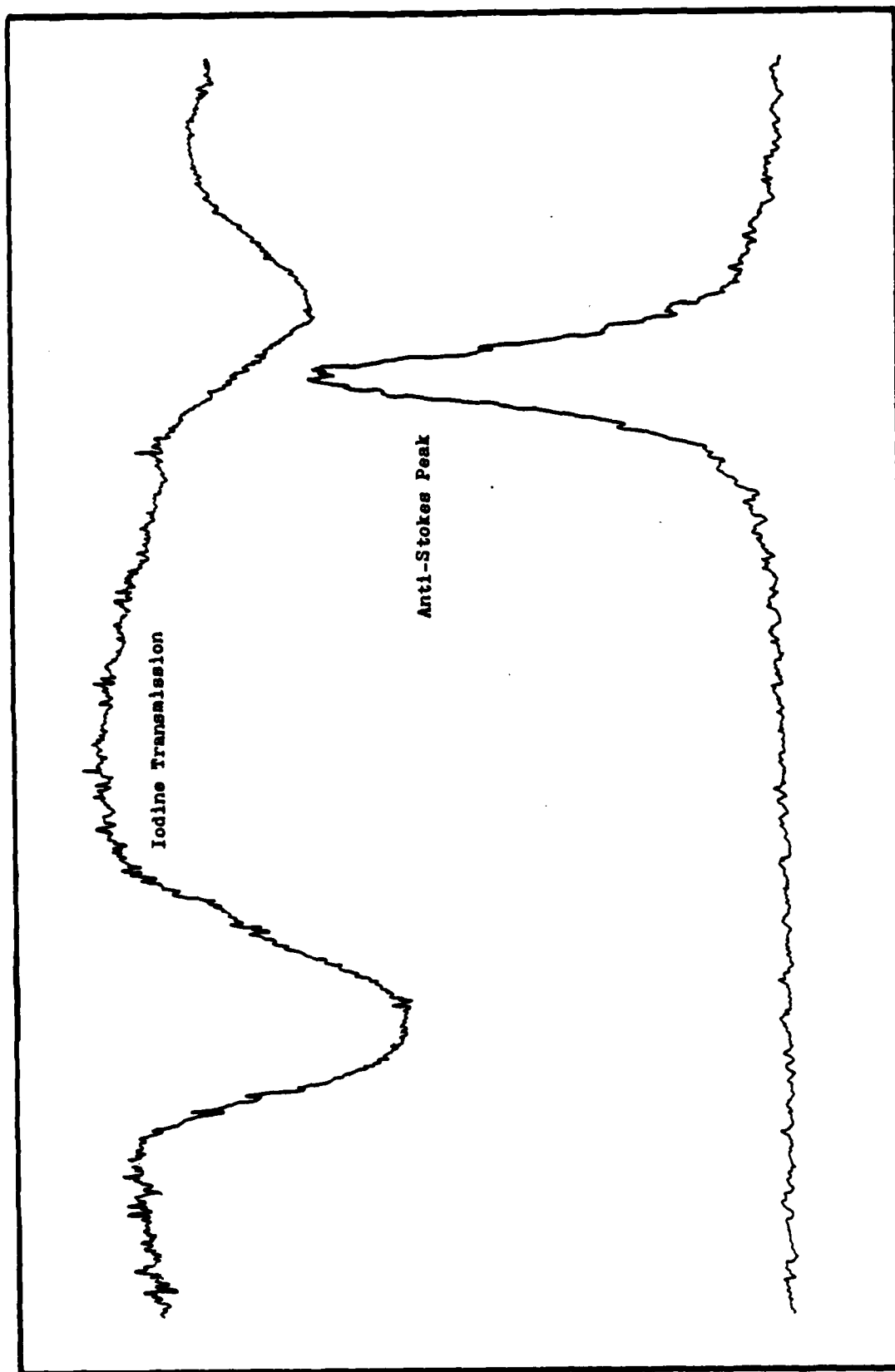


Figure 4. Sample Frequency Strip Chart Recording

VI. Analysis

The data presented in Chapter V has been plotted and analyzed in this chapter to make it more comprehensible. The pressure broadening coefficient, the self diffusion coefficient, and the frequency shift coefficient were determined for each of the observed transitions. For comparison purposes, the pressure in atmospheres was converted to the gas density in amagats, where one amagat is the density of gas at one atmosphere at 0°C (273K). The appropriate conversion is the ratio of 0°C to the temperature of the experiment, which was usually 22°C (295K). Thus, the density in amagats equals 0.925 times the pressure in atmospheres at 22°C.

Linewidth Analysis

The linewidth in the region of pressure that was studied is a function of pressure broadening and Dicke narrowing, as discussed in Chapter 2. In the model in equation (25), the two coefficients that characterize the linewidth are the self-diffusion coefficient (D_0) and the pressure broadening coefficient (a). A nonlinear least squares curve fitting routine was used to find the values of the coefficients that produced the smallest RMS error between the linewidth model and the data points. The linewidth data points for the Q(0) through Q(4) transitions and the curves with the best fit are plotted in Figures 5 through 9, respectively. The error

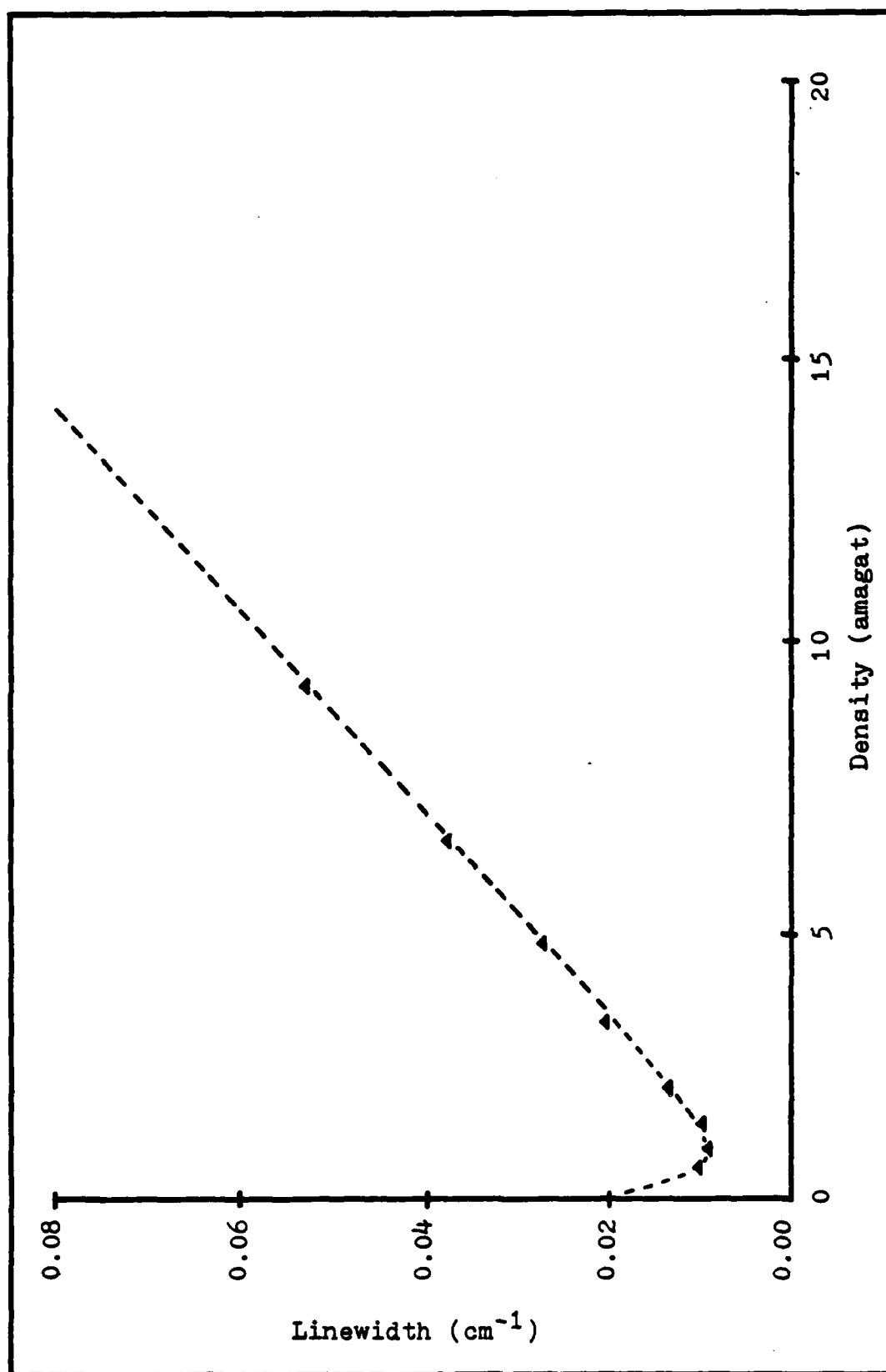


Figure 5. Q(0) Linewidth vs Density

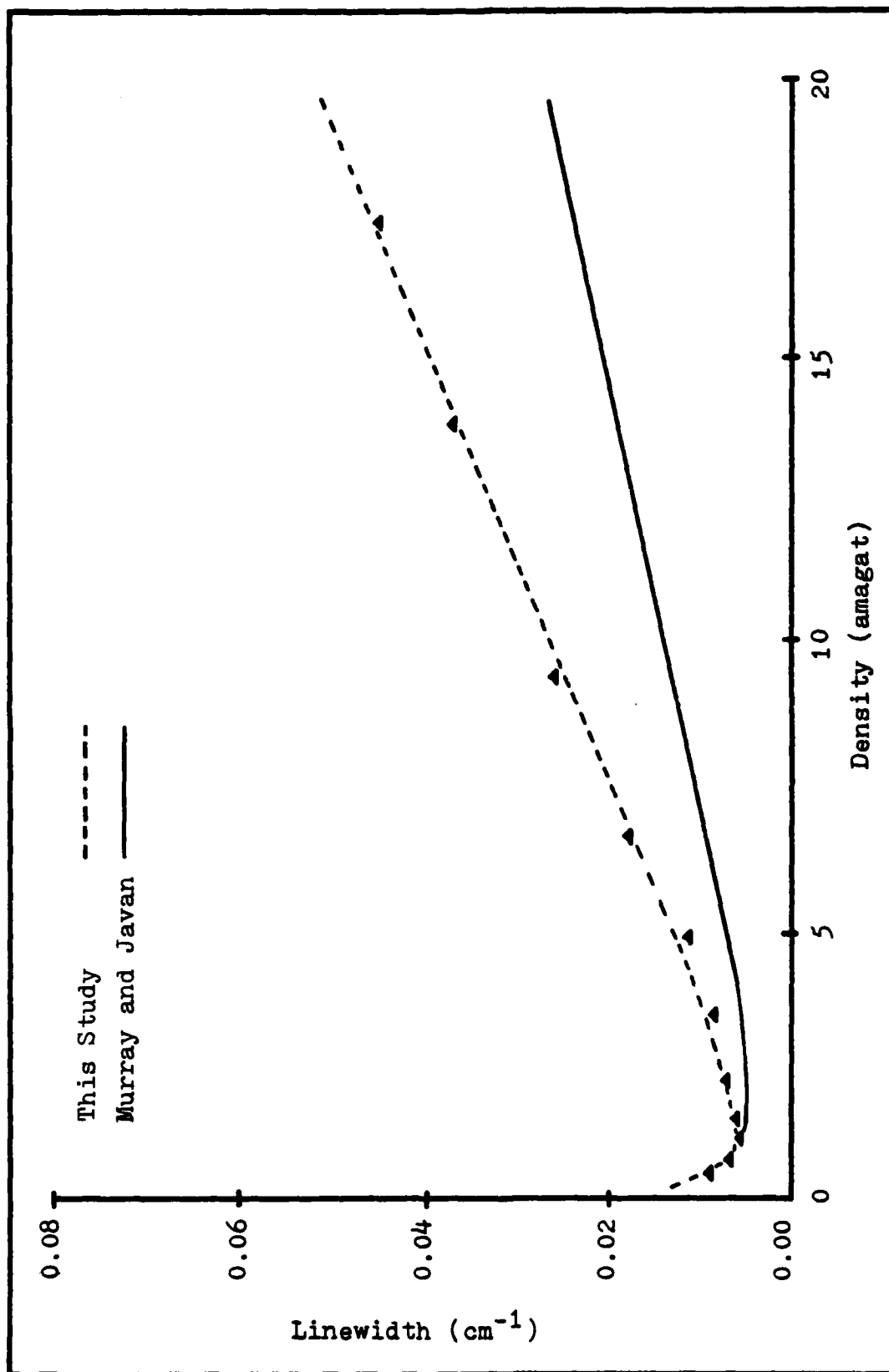


Figure 6. Q(1) Linewidth vs Density

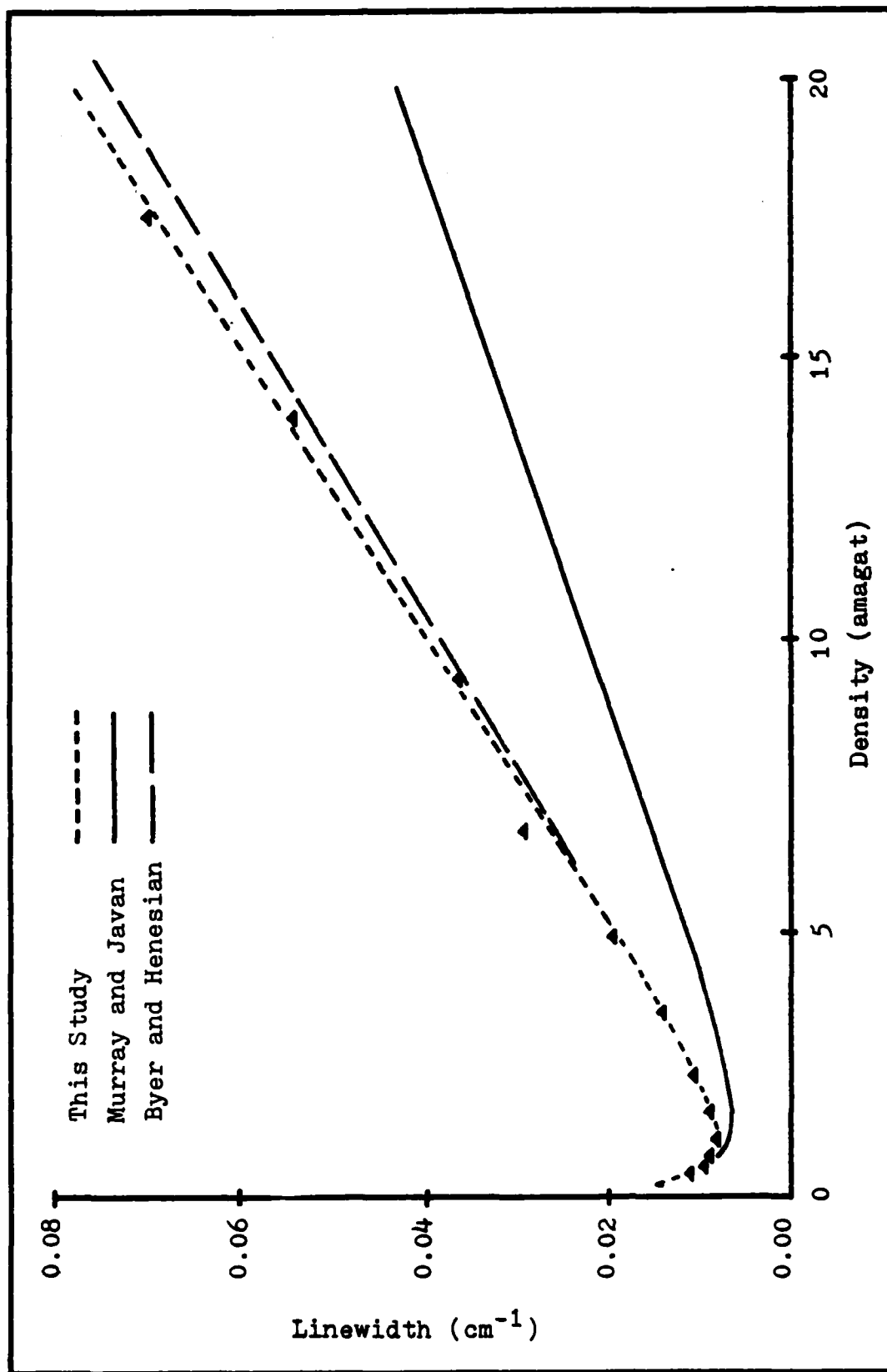


Figure 7. Q(2) Linewidth vs Density

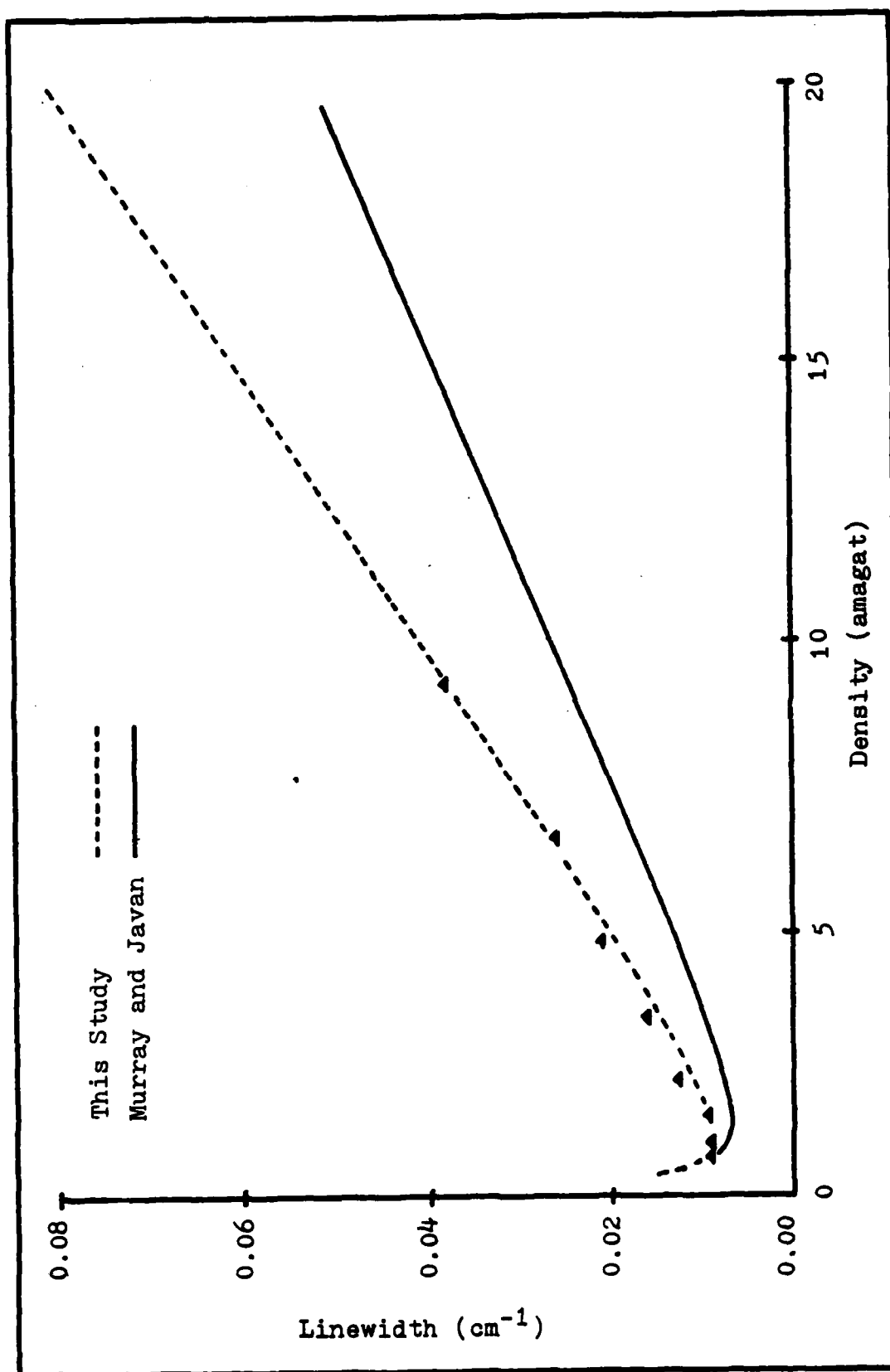


Figure 8. Q(3) Linewidth vs Density

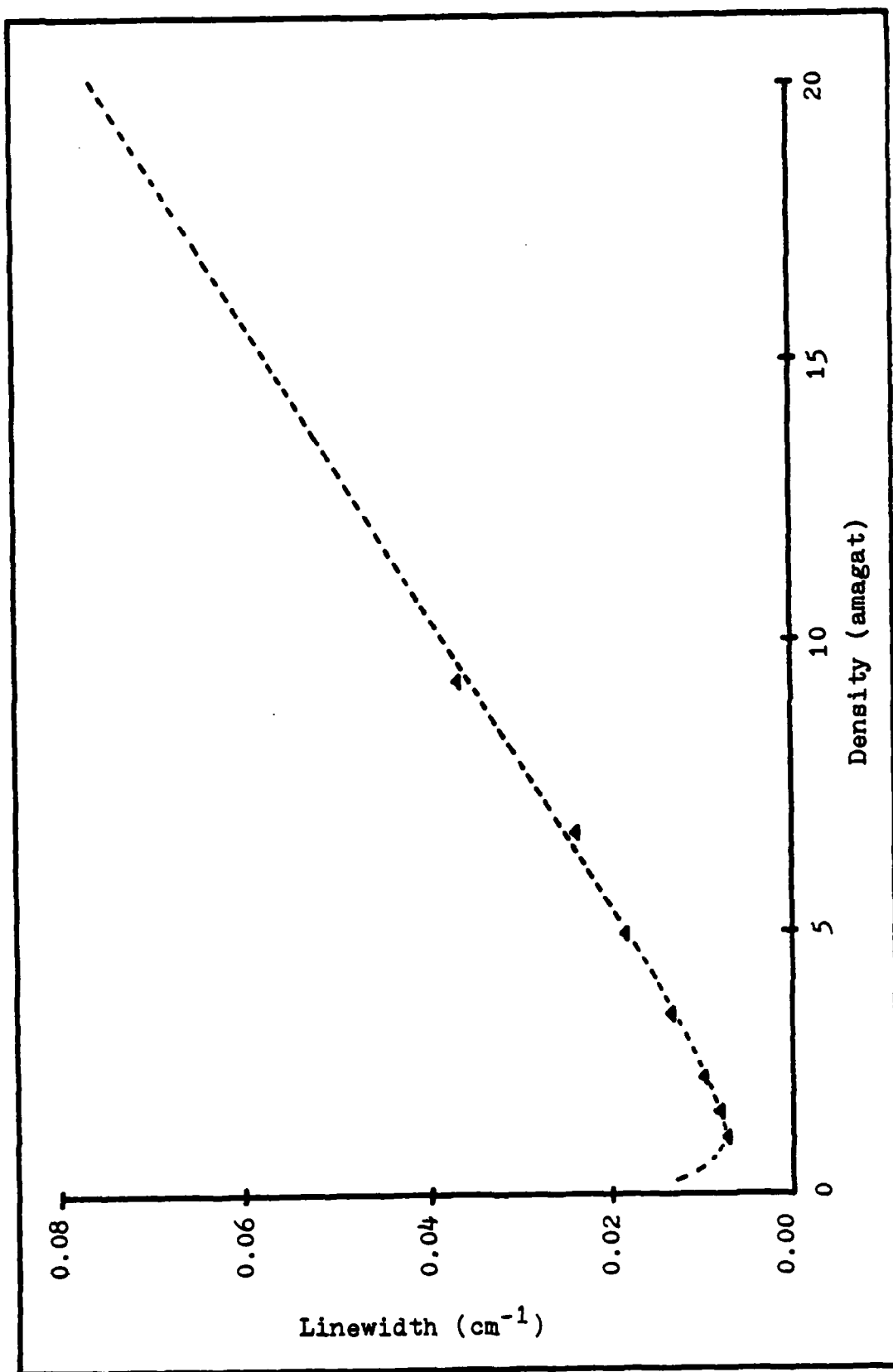


Figure 9. Q(4) Linewidth vs Density

bars are smaller than the symbols that represent the data points, so the error bars are not shown in the figures. The plotted points are the average values of the three runs taken at each pressure for each line. The error bars represent the variation of the linewidth of each individual run about the average value.

The linewidths reported by Murray and Javan,¹⁷ and Byer and Henesian¹⁸ are also shown in Figures 6 through 8. Murray and Javan's linewidth curves for Q(1) through Q(3) are consistently lower than the curves of this work, as shown in Figures 6, 7, and 8. Since all three figures show the same pattern, the difference may be that the two experiments did not use the same technique to make these measurements. Since Byer and Henesian reported their work in atmospheres at room temperature, their data, as shown in Figure 7, have been converted to amagats. It was assumed that their room temperature was 22°C. Byer and Henesian's Q(2) data nearly matches the curve from this study, indicating a close agreement. Figure 10 shows the entire family of curves from this experiment.

Henesian and others have reported two other experiments dealing with the linewidth of the Q(2) transition.^{19,20} In both of these reports, the results were only displayed graphically, making any analytical comparison impossible. However, the linewidths do appear to correspond well with this work.

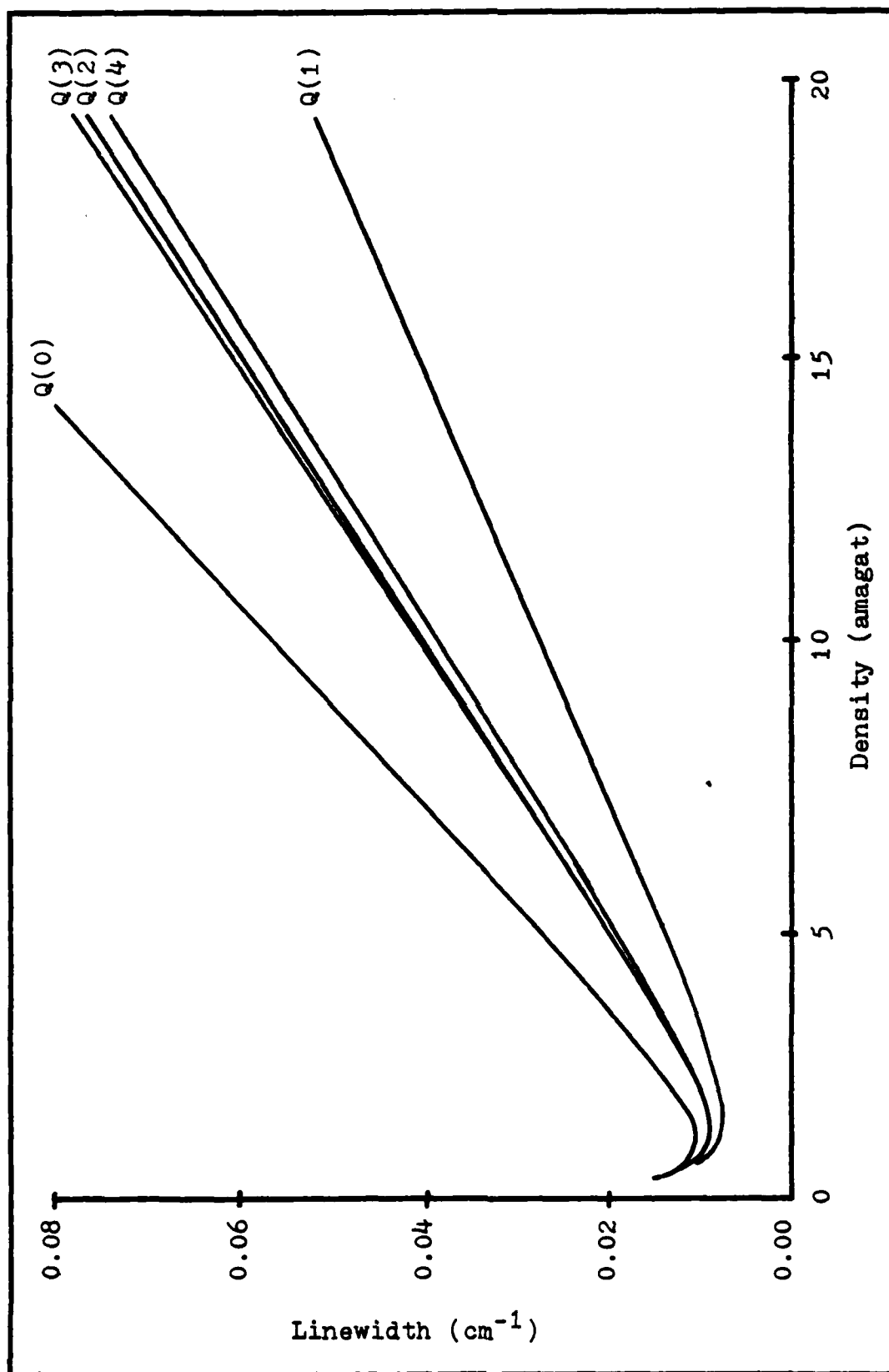


Figure 10. Linewidth of all Transitions vs Density

For a quantitative comparison between this and other work, the pressure broadening and self diffusion coefficients are shown in Table X. While the values of the coefficients of this work are not the same as Murray and Javan's work, the results of this work are more accurate. The RMS errors, δ , of this study are 20 to 30 times smaller than Murray and Javan's RMS errors, indicating a much better fit to the data. In fact, the obviously large error committed by fitting their coefficients to the data points of this study is less than half of their reported RMS error. Although Byer and Henesian did not report an RMS error, the value of their coefficients are close to the numbers from this work.

If the diffusion model of Dicke narrowing were strictly valid, the diffusion coefficients should have the same value for all of the transitions. However, the best fit to the data was obtained with different diffusion coefficients. This is the first known experimental determination of the diffusion coefficient for deuterium; the other reported diffusion coefficients are estimates. Murray and Javan state that their diffusion coefficient is "accurate to perhaps 10%"¹⁷ while Byer and Henesian state "one would estimate" the value that they reported.¹⁸

This work is also the first to report on five Q-branch transitions. Most other researchers have only dealt with the Q(2) line and Murray reported the most lines when he examined Q(1) through Q(3). This study of two unexplored lines

TABLE X

Pressure Broadening and Self Diffusion Coefficients

Transition	This Study			Murray & Javan ¹⁷			Byer & Henesian ¹⁸	
	a	D ₀	δ	a	D ₀	δ	a	D ₀
Q(0)	5.79	1.092	2.3	-	-	-	-	-
Q(1)	2.70	0.860	2.5	1.4	0.952	70	-	-
Q(2)	4.00	0.889	2.9	2.2	0.952	70	3.8	1.02
Q(3)	4.10	1.126	3.7	2.6	0.952	80	-	-
Q(4)	3.87	0.914	2.9	-	-	-	-	-

Comments: a in units of $10^{-3} \text{ cm}^{-1} \text{ amagat}^{-1}$
D₀ in units of $10^{-3} \text{ cm}^2 \text{ amagat s}^{-1}$
δ in units of 10^{-4} cm^{-1}

provides valuable new information. Considering the small range in RMS errors for all the lines, the Q(0) and Q(4) coefficients should be just as accurate as the central three lines.

Transition Frequency Analysis

Measuring the transition frequency of each line and determining its variation with pressure was another part of this study. The transition frequency seems to decrease linearly with an increase in the density of the gas. A linear least squares routine was used to find the best line to fit the data, as that method has been used in earlier work.^{4,17} The model is

$$\omega_v(\rho) = \omega_v(\rho=0) + b\rho \quad (27)$$

where $\omega_v(\rho=0)$ is the reported value of the transition frequency and b is the frequency shift coefficient.

The experimentally determined transition frequencies and the transition frequencies calculated from the Dunham coefficients are displayed in Table XI. The Q(2) transition frequency reported by Byer's group²⁰ is also provided for comparison.

The value of this information cannot be determined until the fit of the least squares routine is examined. The transition frequencies for the Q(0) through Q(4) lines are plotted in Figures 11 through 15, respectively. The data points appear to be scattered and the quality of the fit is

TABLE XI

Transition Frequencies

Transition	This Study	From Dunham Coeff.	Henesian ¹⁸
Q(0)	2993.609	2993.801	-
Q(1)	2991.518	2991.691	-
Q(2)	2987.306	2987.476	2987.2371
Q(3)	2981.005	2981.167	-
Q(4)	2972.631	2972.779	-

Comment : All frequencies in units of cm^{-1}

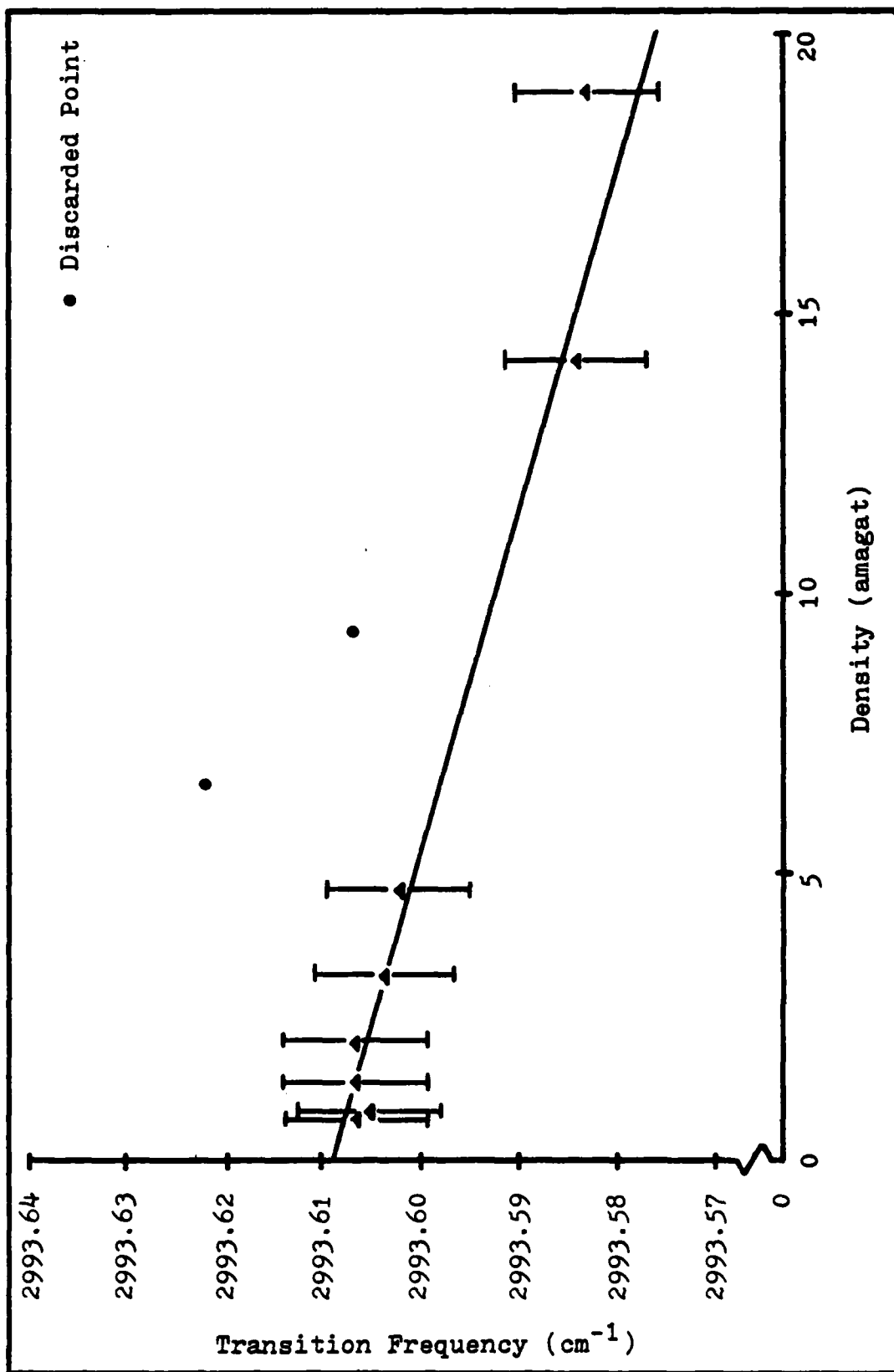


Figure 11. Q(0) Transition Frequency vs Density

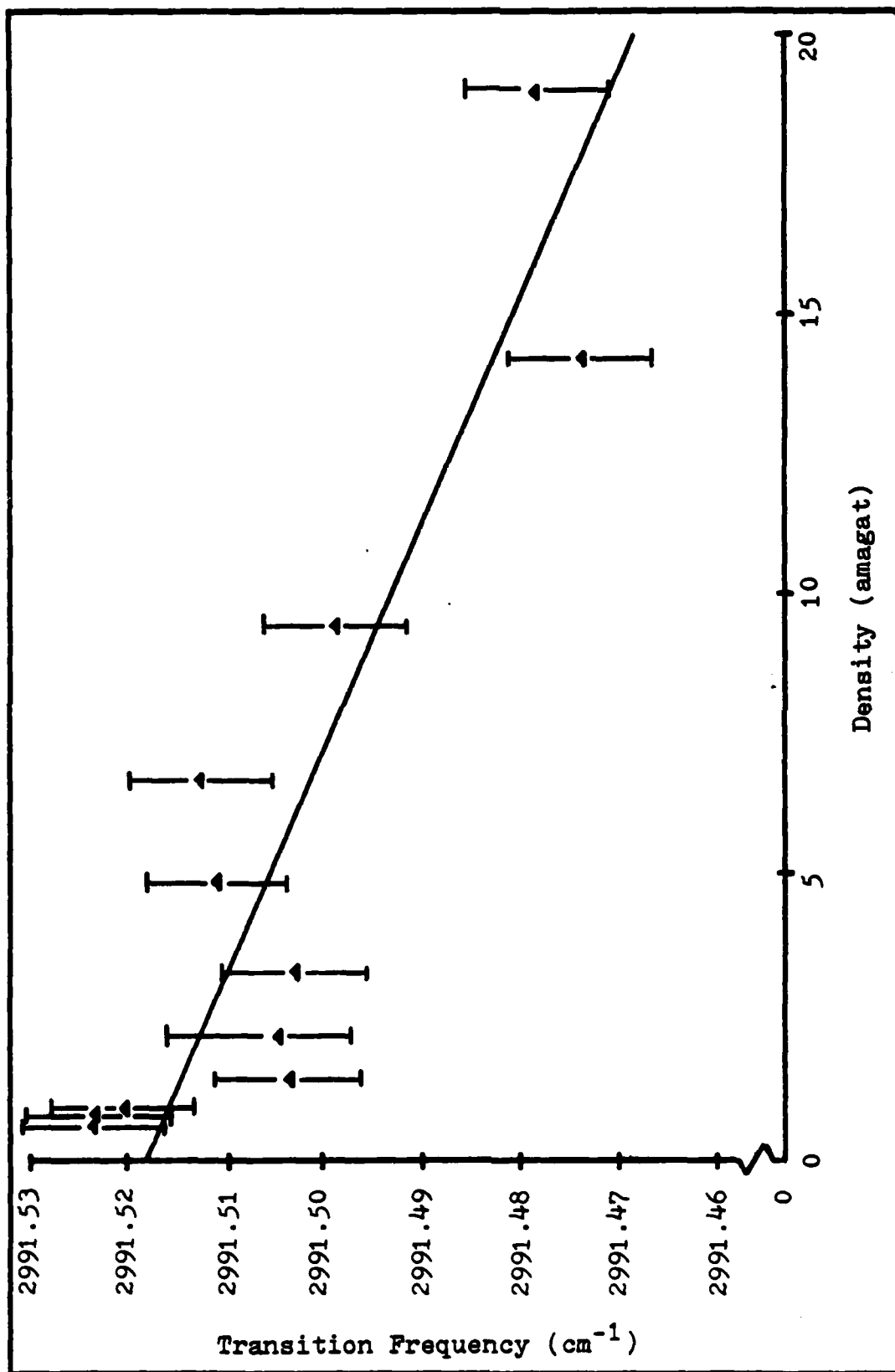


Figure 12. Q(1) Transition Frequency vs Density

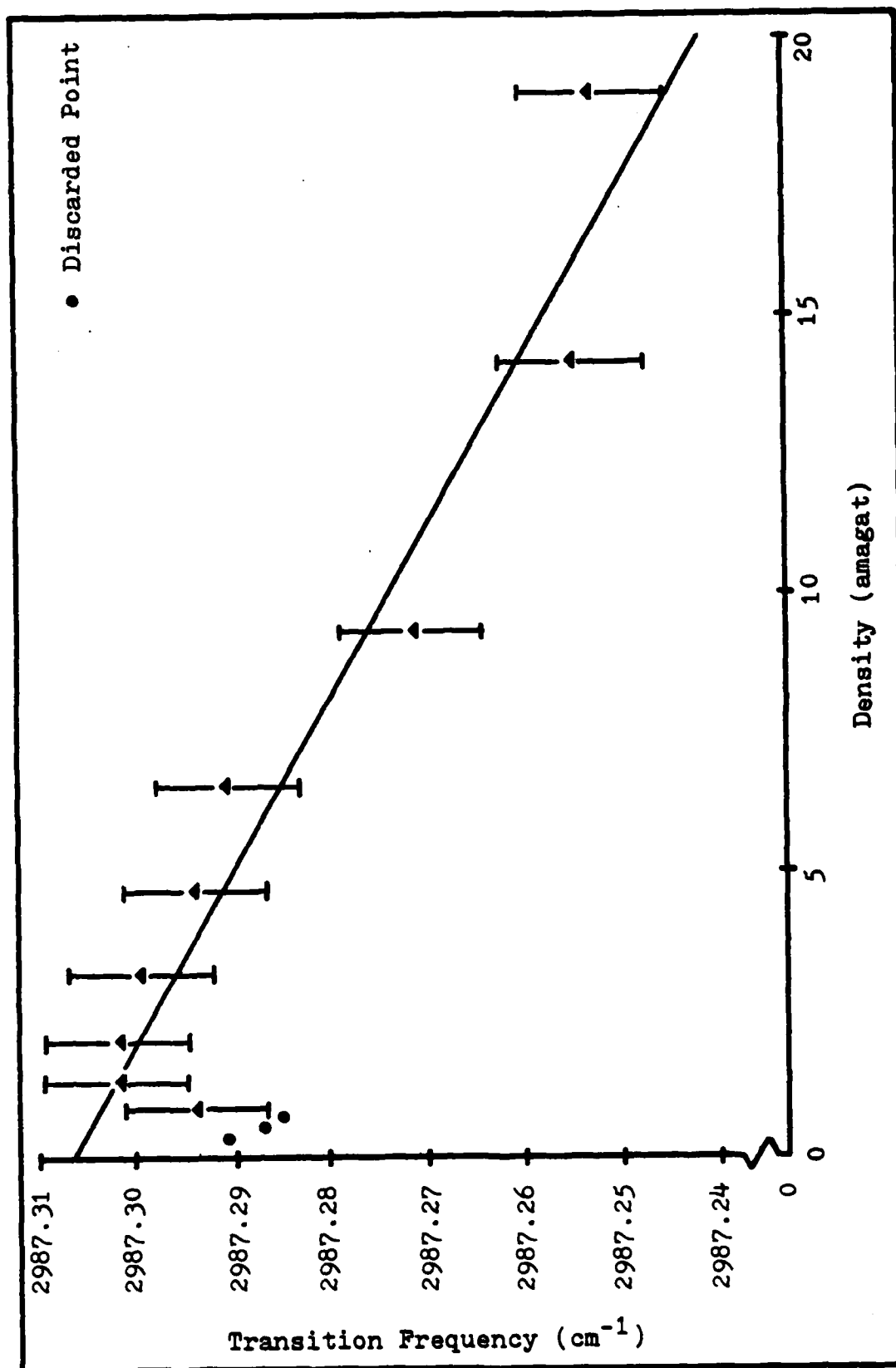


Figure 13. Q(2) Transition Frequency vs Density

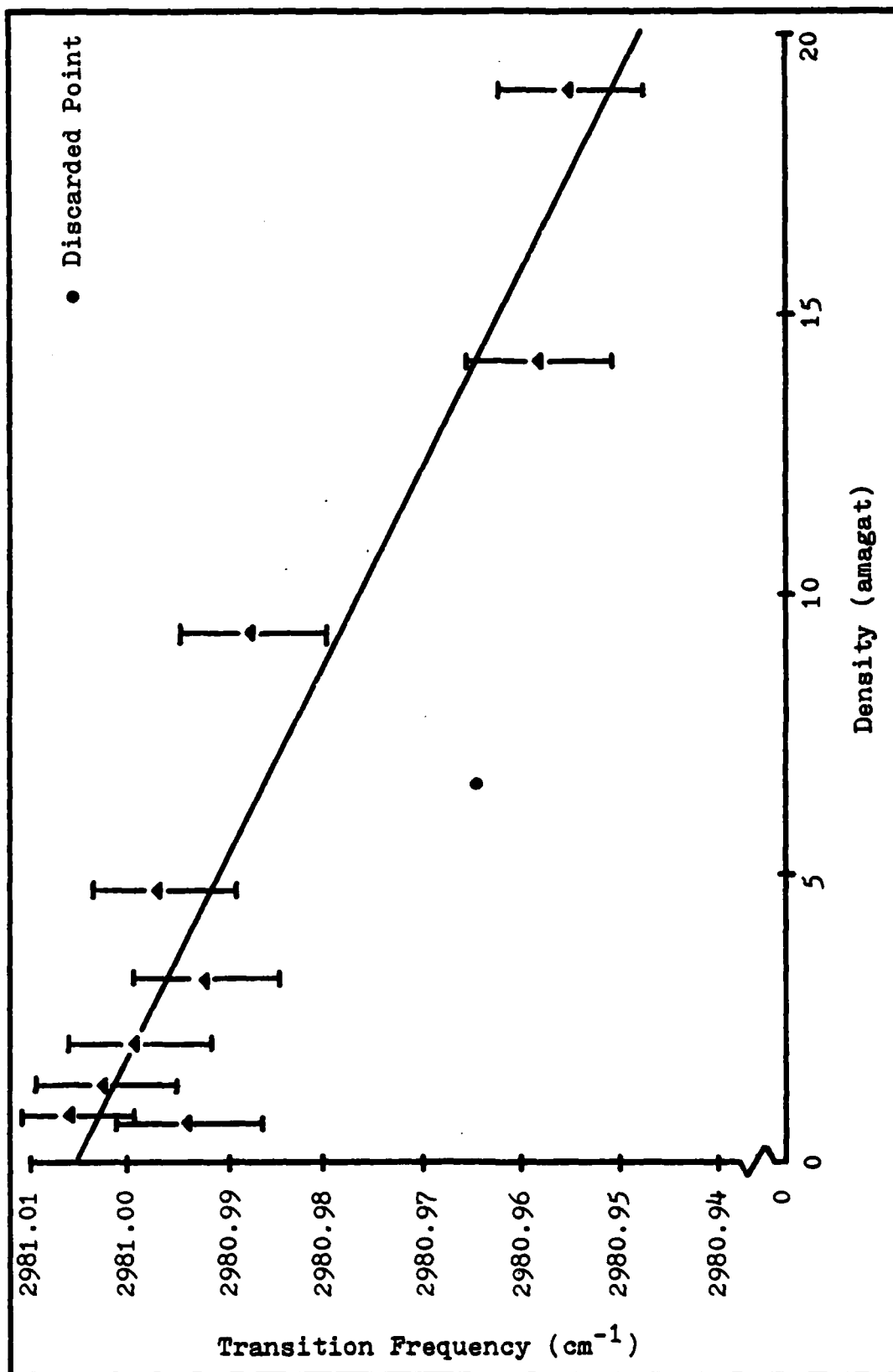


Figure 14. Q(3) Transition Frequency vs Density

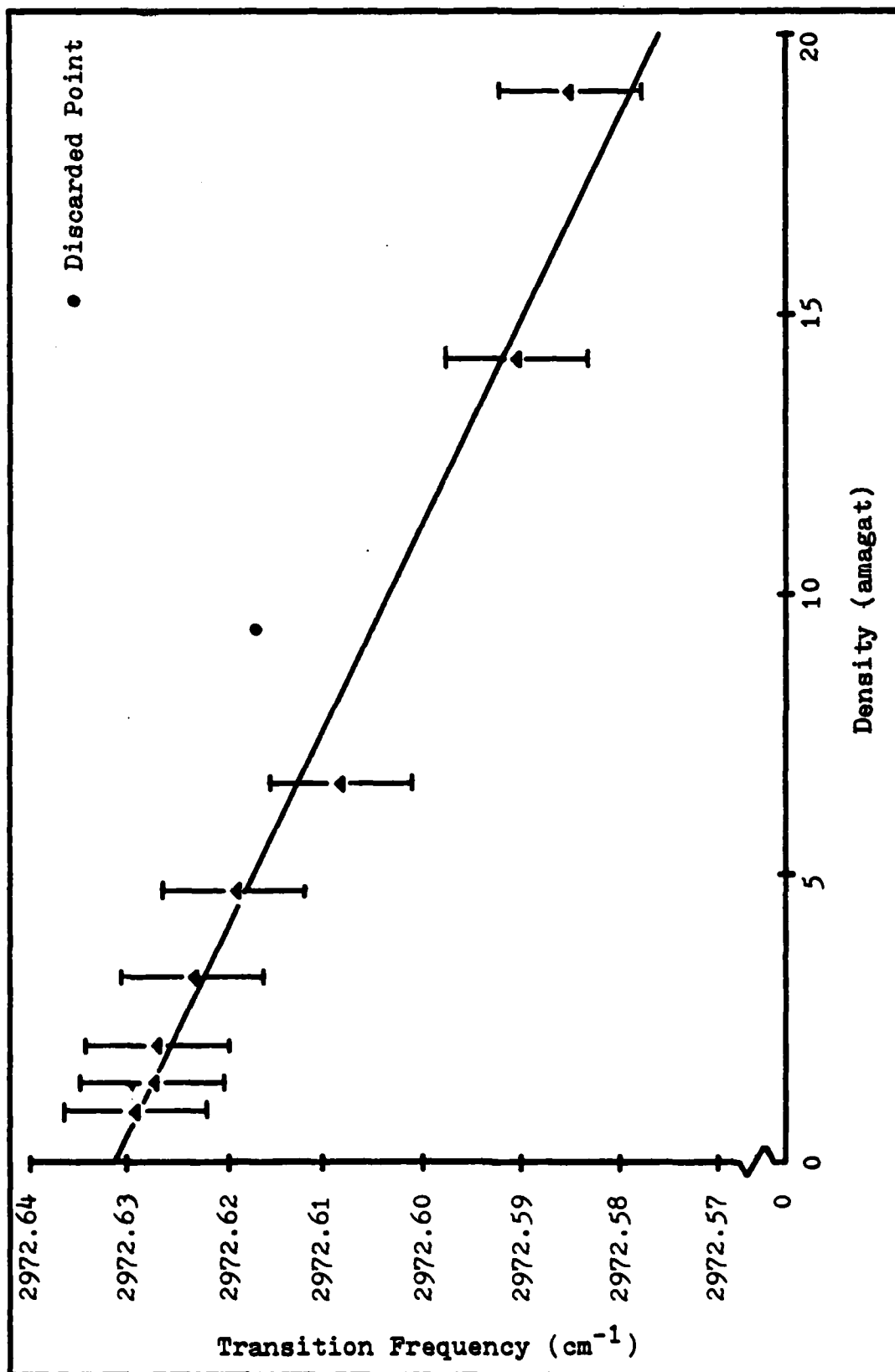


Figure 15. Q(4) Transition Frequency vs Density

not good. In fact, to get this fit, some points were discarded because they were too far from the line and were obviously erroneous. The discarded points are indicated by circles in the figures.

The cause of the scattered data is simple, but the solution is not. The pump beam frequency was established by maximizing the fluorescence from the iodine cell. However, the Doppler-broadened iodine peaks are approximately 700MHz wide, and within 10% of the peak, the iodine lines are up to 450MHz (0.015cm^{-1}) wide. Thus, while the intensity of the fluorescence from the iodine cell was always near its maximum, the laser could have been anywhere in a frequency range approximately 450 MHz wide. This is what caused the large error bars. The frequency problem was not in mode hopping as that would have been noticed. Also, the data that was taken during one day is internally consistent. The problem lies in the laser not coming up on the same frequency every day. Correcting this problem will be difficult without frequency stabilizing the argon ion pump laser.

The frequency shift coefficients are summarized in Table XII, along with Murray and Javan's results.¹⁷ The poor fit created an RMS error that is approximately the same as Murray and Javan's. Thus, the central three lines provide no significant new information. It is not known which results are more accurate. The cause of the RMS

TABLE XII

Frequency Shift Coefficients

Transition	This Study		Murray & Javan ¹⁷	
	b	δ	b	δ
Q(0)	-1.63	1.7	-	-
Q(1)	-2.45	12.6	-1.45	8
Q(2)	-3.21	7.5	-1.7	6
Q(3)	-2.84	8.1	-1.35	-
Q(4)	-2.73	3.3	-	-

Comments : b in units of $10^{-3} \text{ cm}^{-1} \text{ amagat}^{-1}$
 δ in units of 10^{-3} cm^{-1}

errors of $Q(0)$ and $Q(4)$ being lower than the other errors is also unknown. The significant result is that frequency shift coefficients for $Q(0)$ and $Q(4)$, which have never been reported, are now available.

VII. Conclusions and Recommendations

A high spectral resolution cw CARS system was used to measure the linewidths and the transition frequencies of the Q-branch of deuterium. More transitions have been measured in this project than in any other known work. While most researchers have only reported results on the strongest Q(2) transition, and Murray and Javan reported on Q(1) through Q(3), two additional transitions were observed in this experiment, resulting in the Q(0) through Q(4) transitions being reported.

This measurement, which covered between 0.35 and 20 atmospheres at room temperature, produced meaningful results on the linewidth of deuterium. The pressure broadening coefficients are the most accurate yet, and the self diffusion coefficient was experimentally determined on the basis of the diffusion model of Dicke narrowing.

The system was refined during this work to make further studies possible. A gas handling system was developed to control the pressure in the sample cell without removing the cell. The optical alignment was found to be more critical than previously thought, requiring iterative fine tuning of the optics to maximize the anti-Stokes signal. An attempt to monitor the pump laser frequency indicated that the frequency of the laser does not change during one day, but that it does change from day to day. Active frequency stabilization of the pump beam is deemed necessary to

correct this problem and provide better transition frequency measurements.

Since this is only one in a series of projects on this system, some recommendations are appropriate. When scans are performed to determine the high pressure linewidth, the dye laser should be scanned rapidly or the chart paper should run slowly. Either of these operations will make the AS peak more observable and may allow more accurate measurements. To also improve the measurements, the fluorescence, not absorption, should be detected from the iodine cell. With this arrangement, the baseline would not move as the laser power changes. Finally, the anti-Stokes signal should be optimized by iteratively improving the optical alignment before each series of scans. If this is carefully done, the coefficients determined in future experiments will be more accurate, and more transitions may be observed.

Bibliography

1. Eckbreth, A. C. and P. W. Schreiber. "Coherent Anti-Stokes Raman Spectroscopy(CARS): Applications to Combustion and Gas-Phase Diagnostics," Chemical Applications of Nonlinear Raman Spectroscopy, edited by A. B. Harvey. New York: Academic Press, 1981.
2. Roh, W. B. Coherent Anti-Stokes Raman Scattering of Molecular Gases: Final Report, 1 March 1975 - 30 April 1977. Contract F336615-75-C-1116. Systems Research Laboratories Inc., Dayton OH, August 1977 (AD-A050-156).
3. Cleis, R. A., W. B. Roh, and L. P. Goss. "Raman Linewidths of Hydrogen Fluoride Determined by Using Low-Resolution Coherent Anti-Stokes Raman Spectroscopy," Journal of the Optical Society of America B, 1: 774-778 (December 1984).
4. Melton, D. W. and A. M. Toich. Linewidth and Bandwidth Measurements of the Q-branch of H₂ Using CW Coherent Anti-Stokes Raman Spectroscopy. MS thesis. School of Engineering, Air Force Institute of Technology (AU), Wright-Patterson AFB, OH, December 1984.
5. Gustafson, E. K. and R. L. Byer. "Coherent Anti-Stokes Raman Scattering from Small Volumes," Optics Letters, 9: 220-222 (June 1984).
6. Hecht, E. and A. Zajac. Optics. Menlo Park, California: Addison-Wesley Publishing Co., 1974.
7. Roh, W. B. Lecture, PH 7.99, Independent Study. School of Engineering, Air Force Institute of Technology (AU), Wright-Patterson AFB, OH, April 1985.
8. Yariv, A. and P. Yeh. Optical Waves in Crystals. New York: John Wiley and Sons, 1984.
9. Fabelinsky, V. I. and others. "High Resolution CW CARS Spectroscopy of the Q-branch of the ν_2 Band in C₂H₂," Optics Communications, 20: 389-391 (March 1977).
10. Krynetsky, B. B. and others. "High Resolution CW CARS Spectroscopy in D₂ Gas," Optics Communication, 21: 225-228 (May 1977).

11. Roh, W. B., R. F. Weber, and P. W. Schreiber. "Linewidth Determination by Integrated Power Measurement of Coherent Anti-Stokes Raman Scattering," Optics Communications, 27: 142-146 (October 1978).
12. Tolles, W. M. and A. B. Harvey. "Introduction to Nonlinear Phenomena," Chemical Applications of Nonlinear Raman Spectroscopy, edited by A. B. Harvey. New York: Academic Press, 1981.
13. Dicke, R. H. "The Effect of Collisions upon the Doppler Width of Spectral Lines," Physical Review, 89: 472-473 (15 January 1953).
14. Huber, K. P. and G. Herzberg. Molecular Spectra and Molecular Structure: IV. Constants of Diatomic Molecules. Cincinnati: Van Nostrand Reinhold Company, 1979.
15. Gerstenkorn, S. and P. Luc. Atlas du Spectre d'Absorption de la Molécule D'iode 14800-20000 cm⁻¹. Paris: Editions du Centre National de la Recherche Scientifique, 1978.
16. Gerstenkorn, S. and P. Luc. "Absolute Iodine (I₂) Standards Measured by means of Fourier Transform Spectroscopy," Revue de Physique Appliquée, 14: 791-794 (August 1979).
17. Murray, J. R. and A. Javan. "Effects of Collisions on Raman Line Profiles of Hydrogen and Deuterium Gas," Journal of Molecular Spectroscopy, 42: 1-26 (1972).
18. Byer, R. L. and M. A. Henesian. Coherent Anti-Stokes Raman Spectroscopy: Final Report. Contract N00014-75-C-0894. W. W. Hansen Laboratories of Physics, Stanford University, Stanford, CA, March 1977 (AD-A042-273).
19. Henesian, M. A. and others. "Absolute Raman Frequency Measurements of the Q(2) Line in D₂ using CW CARS," Optics Letters, 1: 149-151 (November 1977).

20. Henesian, M. A. and others. "CW High-resolution CAR Spectroscopy of H_2 , D_2 , and CH_4 ," Optics Communications, 18: 225-226 (July 1976).

Vita

Second Lieutenant David A. Russell was born on 26 December 1962 in Rome, New York. He graduated from Fountain Valley High School in Fountain Valley, California in 1980. He attended the University of Washington and earned the degree of Bachelor of Science in Electrical Engineering in June 1984. Upon graduation, he received a commission in the USAF through the AFROTC program and immediately entered the School of Engineering, Air Force Institute of Technology.

Permanent Address: 19425 NE 181st Street
Woodinville, Washington 98072

UNCLASSIFIED

SECURITY CLASSIFICATION OF THIS PAGE

AD-A163946

REPORT DOCUMENTATION PAGE

1. REPORT SECURITY CLASSIFICATION UNCLASSIFIED		1b. RESTRICTIVE MARKINGS	
2a. SECURITY CLASSIFICATION AUTHORITY		3. DISTRIBUTION/AVAILABILITY OF REPORT Approved for public release; distribution unlimited	
2b. DECLASSIFICATION/DOWNGRADING SCHEDULE		5. MONITORING ORGANIZATION REPORT NUMBER(S)	
4. PERFORMING ORGANIZATION REPORT NUMBER(S) AFIT/GEO/ENP/85D-4		7a. NAME OF MONITORING ORGANIZATION	
6a. NAME OF PERFORMING ORGANIZATION School of Engineering	6b. OFFICE SYMBOL (If applicable) AFIT/ENP	7b. ADDRESS (City, State and ZIP Code)	
6c. ADDRESS (City, State and ZIP Code) Air Force Institute of Technology Wright-Patterson AFB, Ohio 45433		9. PROCUREMENT INSTRUMENT IDENTIFICATION NUMBER	
8a. NAME OF FUNDING/SPONSORING ORGANIZATION	8b. OFFICE SYMBOL (If applicable)	10. SOURCE OF FUNDING NOS.	
8c. ADDRESS (City, State and ZIP Code)		PROGRAM ELEMENT NO.	PROJECT NO.
11. TITLE (Include Security Classification) See Box 19		TASK NO.	WORK UNIT NO.
12. PERSONAL AUTHOR(S) David A. Russell, 2d Lt, USAF			
13a. TYPE OF REPORT MS Thesis	13b. TIME COVERED FROM _____ TO _____	14. DATE OF REPORT (Yr., Mo., Day) 1985 December	15. PAGE COUNT 73
16. SUPPLEMENTARY NOTATION			
17. COSATI CODES		18. SUBJECT TERMS (Continue on reverse if necessary and identify by block number)	
FIELD	GROUP	SUB. GR.	
20	06	Coherent Anti-Stokes Raman Spectroscopy	
07	04	Raman Spectroscopy Molecular Spectroscopy	
		Deuterium Stable Isotopes	
19. ABSTRACT (Continue on reverse if necessary and identify by block number)			
Title: HIGH RESOLUTION COHERENT ANTI-STOKES RAMAN SPECTROSCOPY OF DEUTERIUM GAS			
Thesis Advisor: Won B. Roh, PhD Associate Professor of Engineering Physics			
Approved for public release: IAW AFR 190-1. Lynn E. WOLAVER 16 JAN 86 Dean for Research and Professional Development Air Force Institute of Technology (AFIT) Wright-Patterson AFB OH 45433			
20. DISTRIBUTION/AVAILABILITY OF ABSTRACT UNCLASSIFIED/UNLIMITED <input checked="" type="checkbox"/> SAME AS RPT. <input type="checkbox"/> DTIC USERS <input type="checkbox"/>		21. ABSTRACT SECURITY CLASSIFICATION UNCLASSIFIED	
22a. NAME OF RESPONSIBLE INDIVIDUAL Won B. Roh, Associate Professor of Engineering Physics		22b. TELEPHONE NUMBER (Include Area Code) (513) 255-2012	22c. OFFICE SYMBOL AFIT/ENP

UNCLASSIFIED

SECURITY CLASSIFICATION OF THIS PAGE

High resolution cw coherent anti-Stokes Raman spectroscopy (CARS) was performed in molecular deuterium gas. Single mode argon ion and ring dye lasers were used to make accurate measurements of the Raman linewidths of the $Q(0)$ through $Q(4)$ transitions. These lines were examined at room temperature at pressures ranging from 0.35 to 20 atmospheres. The pressure broadening coefficient and the self diffusion coefficient of each line were obtained in this study and compared with other work. Additionally, the transition frequency of each line was measured and the frequency shift coefficients were obtained.

UNCLASSIFIED

SECURITY CLASSIFICATION OF THIS PAGE

END

FILMED

3-86

DTIC